Applied Thermal Engineering 290 (2026) 129920

Contents lists available at ScienceDirect

Applied Thermal Engineering

journal homepage: www.elsevier.com/locate/ate

Research Paper

Comprehensive energy, exergo-economic, and exergo-environmental (5E) assessment of a novel electric vehicle battery cooling system layout

Mehdi Aliehyaei [a,b], Vincenzo Bianco [c], Mattia De Rosa [a,d,*]

[a] Department of Mechanical, Energy, Management and Transportation Engineering (DIME), University of Genoa, Via All'Opera Pia 15/A, 16145, Genova, Italy
[b] Pardis Branch, Islamic Azad University, Pardis New City, Iran
[c] Dipartimento di Ingegneria, Università degli Studi di Napoli "Parthenope", Isola C4 Centro Direzionale, Napoli, 80143, Italy
[d] International Centre of Energy Resource Management (iCERM), Italy

ARTICLE INFO

Keywords:
Battery cooling system
Thermal modeling
Exergo-economic
Exergo-environmental
Design optimization

ABSTRACT

With the increasing energy density of batteries in electric vehicles (EVs), the design of battery thermal management systems with high energy performance and reduced economic and environmental costs has become a critical challenge. However, most previous studies have focused mainly on energy or exergy analyses, while comprehensive frameworks simultaneously incorporating economic and environmental aspects remain limited. In this study, a novel integrated thermal management system is developed to simultaneously control the temperature of the battery pack, cabin, and electric motor. The system is evaluated using a comprehensive five-dimensional (5E) framework, including energy, exergy, economic, exergo-economic, and exergo-environmental analyses. A detailed thermodynamic model of the proposed system is developed and validated against experimental data, showing deviations below 6% for key performance indicators. Under baseline operating conditions, the system achieves a coefficient of performance (COP) of 3.81, while the overall exergy efficiency is 5.5%, revealing a significant gap between energy quantity and energy quality. Exergy destruction analysis indicates that the evaporator and condenser are the dominant sources of irreversibility, with the condenser accounting for approximately 80% of the total capital cost. The specific cooling cost is estimated as 0.055 US$/kWh. Parametric analyses demonstrate that optimal thermodynamic and economic performance is obtained at mid-range battery state of charge (SOC ≈ 0.65–0.75). A comparative assessment of alternative refrigerants (R152a, R1234yf, and R513A) shows that R152a provides the highest COP (≈ 4.0), whereas R1234yf offers superior environmental performance due to its ultra-low global warming potential. The results highlight the effectiveness of the proposed 5E framework in identifying dominant inefficiencies and trade-offs, and provide practical guidance for the thermodynamic design, refrigerant selection, and sustainable optimization of next-generation EV thermal management systems.

1. Introduction

In recent years, the increase in fossil fuel prices and growing concerns about environmental pollution have led to a significant growth in the development of electric vehicle (EV) and hybrid electric vehicle (HEV) technologies. These vehicles have been proposed as a suitable alternative to combustion vehicles in many countries due to their high energy efficiency, low emissions, diversity of power sources, and quiet operation. They can also balance the distribution network by connecting to the electricity grid [1].

Despite these advantages, challenges such as long and frequent charging times, insufficient acceleration, and limited driving range still prevent their commercial expansion. One of the main reasons for these limitations is the lack of widespread development of charging infrastructure and the need to optimally use the energy stored in the vehicle, which is directly related to the performance of energy storage systems [2,3].

The battery plays a key role in electric and hybrid vehicles, and the performance, range, acceleration, safety, and overall cost of the vehicle depend on its technical characteristics and efficiency. To achieve higher power, more current must pass through the cells, which, according to Ohm's law, leads to the generation of significant heat. If not managed, this heat can dangerously increase the battery temperature. High temperatures not only reduce the operating life of the battery and its capacity but also increase the likelihood of phenomena such as thermal

* Corresponding author at: Department of Mechanical, Energy, Management and Transportation Engineering (DIME), University of Genoa, Via All'Opera Pia 15/A, 16145, Genova, Italy.
E-mail address: mattia.derosa@unige.it (M. De Rosa).

https://doi.org/10.1016/j.applthermaleng.2026.129920
Received 13 September 2025; Received in revised form 4 January 2026; Accepted 21 January 2026
Available online 30 January 2026

runaway and fire. This is especially relevant when the temperature distribution among the cells is not uniform, as a temperature difference of more than 5 degrees Celsius can disrupt the charging and discharging process. Therefore, managing operating temperature within the optimal range (between 20 and 40 degrees Celsius) is crucial [4].

Given the temperature dependence of lithium-ion battery performance, designing an effective battery thermal management system (BTMS) in electric vehicles is a fundamental requirement. In the absence of such a system, hazards such as internal short circuits and even battery explosions may occur. Therefore, battery thermal systems must be able to provide features such as fast response, high safety, low weight, compact design, easy maintenance, and accurate temperature control [5–7].

Today, various methods have been proposed for thermal management, each with its advantages and limitations. One of the simplest and most common is air cooling, which can be used either actively or passively. The active method has higher thermal efficiency, but it is more expensive to build and maintain, while the passive method remains popular due to its simplicity, light weight, and low cost [8,9]. Liquids are more effective at cooling than air because of their better thermal properties. The active method has higher heat transfer rates but it is more energy intensive, while the passive method is simpler, safer, and less energy intensive [10,11].

Another effective method for battery thermal management is represented by Phase-change materials (PCMs), which can support maintaining the proper temperature of the battery by exploiting the PCM's latent heat as a passive method. These systems operate without the need for electricity, pumps, or fans, occupy little space, and exhibit good safety and thermal stability. However, their low thermal conductivity and the potential for leakage are the most significant challenges. Paraffin is one of the most commonly used materials in this method [8,12].

Heat pipes are also known as an effective option in heat management. These devices transfer heat with high efficiency without the need for electricity and through the process of evaporation and condensation of the internal fluid. Due to their very high equivalent thermal conductivity and compact structure, this method is widely used in hybrid designs [13].

The thermoelectric method has also been proposed in recent years for controlling the temperature of batteries. These systems consist of modules that can reduce the temperature of the battery pack through the Peltier effect. Their advantages include the absence of moving parts, quiet operation, zero greenhouse gas emissions, and low maintenance. However, the technology has limitations due to its low efficiency and the need to remove heat from the hot side of the module [8,13].

Furthermore, compression refrigeration cycles (similar to the air conditioning system in a car) are also an accurate and efficient method to cool the battery. Although this method has high efficiency, it is more often used in special applications due to its higher complexity and cost [8,12,13].

The use of hybrid systems in battery thermal management is a novel and effective approach to address multiple requirements of performance, safety, and thermal stability. Using the complementary properties of different components, these systems can overcome the structural limitations, low heat transfer, or high energy consumption of individual systems. For example, combining PCM with air can provide thermal stability and heat storage with a simple structure, while combining liquid with a heat pipe enables rapid heat transfer with a compact structure [8,12,13].

Hybrid systems provide greater design flexibility in response to temperature changes and variable battery thermal loads, which is very important in the real-world operation of electric vehicles. These systems also have multi-criteria optimization capabilities and can be considered a suitable option for industrial development, considering energy, cost, and environmental criteria. As a result, a detailed analysis of these systems with a comprehensive approach is an important step towards designing a new generation of thermal management systems for electric vehicle batteries.

However, for an accurate and multidimensional evaluation of the performance of battery cooling systems in electric vehicles, a comprehensive analysis known as 5E (including energy, exergy, economy, exergo-economic, and exergo-environmental) is of particular importance. Instead of focusing solely on heat transfer or energy consumption, this approach examines all functional, economic, and environmental dimensions of the system in an integrated manner. Through this analysis, it can be determined how much input energy is used (exergy analysis), which parts of the system have the most energy loss or destruction, how investment and operating costs are justified, and what impact they will have on pollutant emissions and environmental sustainability.

In the context of battery cooling systems, this type of analysis helps to select the best configuration in terms of efficiency, cost, and environmental compatibility, and to make engineering and industrial decisions based on quantitative and real data. As a result, 5E analysis is a key tool for designing and optimizing next-generation thermal management systems in electric vehicles. Several studies have investigated different battery cooling approaches; however, important unresolved problems remain due to the lack of a comprehensive 5E framework. First, existing studies do not quantify the true economic cost of exergy destruction in each component, making it unclear which subsystem (e.g., condenser, compressor, or evaporator) imposes the highest avoidable cost. Second, previous research rarely evaluates battery, cabin, and motor cooling in an integrated configuration, leaving the coupled thermodynamic and economic interactions among these subsystems unexplored. Third, no prior study has assessed how operational variables – such as, battery state of charge (SOC) and thermal load – affect cooling costs, exergy efficiency, and system-level environmental impacts. The present work addresses these specific gaps by developing a fully integrated 5E assessment for an EV thermal management system.

Hamut et al. [1] analyzed the thermal management system (TMS) in extended-range electric vehicles under high-temperature conditions using exergy analysis. The results showed that the energy COP ranged from 1.8 to 2.4, while the exergy COP ranged from 0.26 to 0.39, with ambient temperature identified as a key factor influencing exergy performance. Similarly, Lee et al. [14] compared thermal management strategies for electric vehicles (EVs) in cold climates and found that the heat pump (HP) system outperforms positive temperature coefficient (PTC) heaters and hybrid approaches in terms of energy and exergy efficiency.

Togun et al. [15] provide a comprehensive review of battery thermal management systems in electric vehicles; they examine a variety of cooling methods, including air, liquid, PCM, heat pipe, and hybrid systems, and show that liquid cooling and a combination of active–passive methods perform best for reducing temperature and extending battery life. The research also highlights the role of emerging technologies, such as artificial intelligence for predictive temperature control and improving stability and safety.

Wang and Ruan [16] investigated an integrated thermal management system (ITMS) – defined as a combined system of battery cooling and cabin air-conditioning – based on a two-phase pumped cooling and ventilation system for electric vehicles (EVs) was developed. The results showed that radiator cooling consumes only about 3% of the energy of the chiller cooling mode, while the chiller performs better under harsh conditions, indicating the optimization potential of ITMS.

In a study by Wankhede et al. [17], the performance of an air-cooled system for lithium-ion batteries in student formula cars was investigated. The results showed that at an air velocity of 17 m/s, the battery temperature remained within a safe range of 30–40°C, indicating the high potential of air-cooled systems in improving thermal stability and reducing the risk of thermal runaway. Harshit Pandey et al. [18] optimized an air-cooling system for lithium titanate oxide batteries, reducing the average temperature to 38.37°C and achieving

16.4% and 14.57% reductions in average and maximum battery temperatures, respectively. An absorption cooling system is proposed by Habash et al. [19] for an electric bus, which uses the waste heat of the engine as an energy source. By using a silica gel/ethanol pair, the coefficient of performance (COP) of the cooling system increased by about 9%, which improved battery health and increased the vehicle's driving range.

Kumar et al. [20] investigated cylindrical lithium-ion battery cooling using a 3E approach. Among aluminum, PCM, and foam+PCM packages with hybrid nanofluid, the aluminum pack achieved the highest thermal and exergy efficiency, while foam+PCM offered better temperature uniformity and long-term savings despite a higher initial cost.

In the study by Zong et al. [21], a novel R744-based thermal management system called Enhanced Parallel Cooling (EPC) was developed for electric vehicles. The results showed that this system has the potential to improve the efficiency and performance of electric vehicles by increasing the cooling capacity by up to 27.8% and improving the driving range by up to 14.6 km. Song et al. [22] developed a carbon dioxide (CO_2) heat pump-based thermal management system (TMS) for electric vehicles (EVs), tested under World Light Vehicle Test Cycle (WLTC) conditions. They showed that optimal pressure and vapor quality control improve the coefficient of performance (COP), reduce exergy destruction, and enhance battery temperature uniformity by up to 10%.

In a study by Wahab et al. [23], single-phase immersion cooling was investigated for lithium-ion batteries. The results showed that this method can improve the safety, lifespan, and efficiency of electric vehicle batteries by enhancing temperature uniformity by 47.7% and reducing the peak temperature at a discharge rate of 8C. In the study by Sadar et al. [24], an advanced battery thermal management system (BTMS) using thermoelectric coolers (TEC) and transformer oil-based liquid immersion cooling (LIC) was proposed. The results showed that the LIC method significantly reduced the battery temperature compared to natural and forced convection, while in heating mode, it was possible to preheat the battery from −25°C to 0°C, ensuring safe operation and battery service life. An electrochemical–thermal model combined with Computational Fluid Dynamics (CFD) simulation was developed by Adeniran et al. [25] to optimize the immersion cooling system for lithium-ion batteries. Among different dielectric fluids and module designs, the optimized U-type module showed reduced pressure drop and volume, while maintaining temperature uniformity within an acceptable range. These results emphasize the importance of balancing cost, safety, and performance. Finally, the integration of phase-change materials (PMS) with liquid cooling was investigated by Wu et al. [26] for battery performance at high discharge rates. The optimized design, including a three-bent S-shaped channel and multi-cell PCM encapsulation, reduced the peak temperature to 47.5°C and improved temperature uniformity, ensuring thermal safety under 5C discharge conditions.

In this context, the novelty of the present study lies in advancing an integrated thermal management system capable of simultaneously conditioning the battery pack, electric motor, and cabin within a unified architecture. Such a system-level integration has not been examined in previous EV thermal management studies. In addition, this work delivers the first comprehensive 5E assessment applied to an integrated EV cooling architecture, providing new insights into subsystem interactions, exergy destruction costs, and environmental impacts.

The main innovations and distinctions of the present research compared to previous studies can be summarized in the following axes:

- **Comprehensive five-dimensional (5E) analysis for the first time in EV battery thermal management**: most of the existing studies have focused exclusively on energy analysis, and in limited cases, a combined energy and exergy analysis has been considered. Such approaches cannot fully capture the multifaceted behavior of the system. In the present study, a comprehensive framework is introduced that simultaneously addresses five key dimensions: energy, exergy, economic, exergo-economic, and exergo-environmental (5E). This multidimensional perspective provides a holistic evaluation of system performance, covering not only thermodynamic efficiency but also cost distribution and sustainability aspects.
- **Development of a comprehensive exergo-economic framework based on realistic cost data**: economic analyses in previous studies were generally limited to approximate estimations of investment and operating costs. In contrast, the present study develops a robust exergo-economic framework that incorporates real cost data for each component, including investment costs, interest rates, equipment lifetime, and operating expenses. This enables precise evaluation of the specific cooling cost (SCC) and quantification of the economic impact of exergy destruction in each component, thus providing valuable insights for industrial applications and investment decisions.
- **Integration of environmental assessment based on exergy principles**: environmental and sustainability aspects have often been neglected in previous EV thermal management research. In this study, a comprehensive exergo- environmental analysis is introduced, in which the environmental damage index (EDI) is calculated for each component based on its exergy consumption and environmental footprint. This novel perspective emphasizes that system optimization should not only account for technical and economic factors but also consider environmental impacts, thereby contributing to sustainable vehicle design.
- **Detailed thermodynamic and fluid flow modeling of system components**: many previous studies have relied on oversimplified models, in which the main components were considered as black-box units with no attention to internal thermal and hydraulic behavior. In this work, detailed modeling of each system component – including the compressor, evaporator, condenser, expansion valve, battery, motor, and cabin – has been carried out, with explicit consideration of refrigerant and coolant flow paths. This level of detail allows tracking of temperature, pressure, enthalpy, and exergy variations across the system, leading to more accurate identification of losses and optimization opportunities.
- **Integrated thermal management of multiple vehicle subsystems**: whereas most previous studies have focused solely on battery cooling, the proposed system provides an integrated solution that simultaneously manages the thermal needs of the battery pack, motor, and cabin. This integrated design improves the overall efficiency of the vehicle thermal management system, reduces operational complexity, and eliminates the need for multiple independent cooling loops.
- **Introduction of new performance indicators for system evaluation**: in addition to conventional indicators such as the coefficient of performance (COP) and exergy efficiency, new indicators are introduced in this study, including the specific cooling cost (SCC) and the environmental damage index (EDI). These indicators enable multi-dimensional assessment of the system and allow more comprehensive comparisons with other configurations in the literature.

2. Materials and methods

2.1. Process description

Fig. 1 shows the thermal management system analyzed in the present work. The combined system is designed to maintain the optimal operating range for the critical components of the electric vehicle, including the batteries, electric engine, and vehicle cabin. The evaporator of the refrigeration system plays a key role in providing the cooling

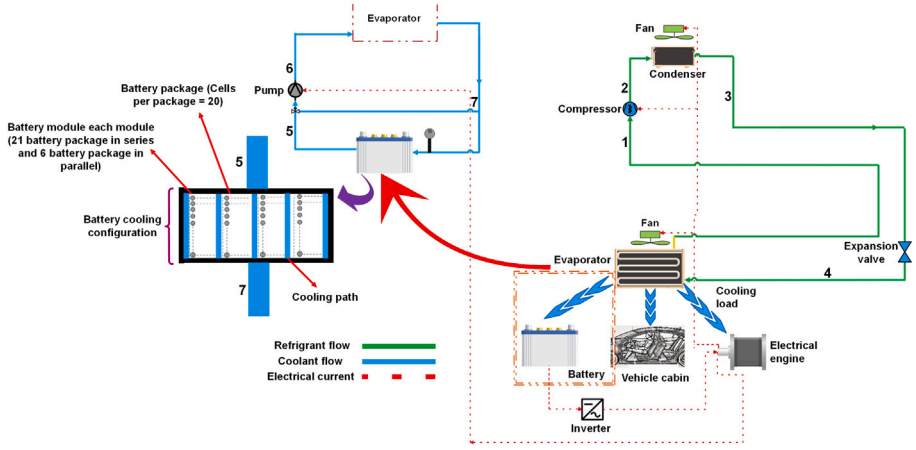

Fig. 1. Schematic diagram of the proposed integrated electric vehicle thermal management system.

required to cool the electric engine and the vehicle cabin. In contrast, battery cooling is mainly entrusted to the liquid cooling loop.

The refrigeration process in this system begins with the compressor (1), where the refrigerant is compressed from a low-pressure vapor state into a high-pressure vapor. This hot vapor then enters the condenser (2), where it transfers its heat to the outside environment using a fan and turns into a high-pressure liquid. The liquid refrigerant is then directed through path (3) to the expansion valve (4). At this point, the pressure and temperature of the refrigerant suddenly decrease, and the refrigerant enters the evaporator (4).

In the evaporator, the low-pressure refrigerant is responsible for absorbing heat from various components, including the electric motor, the vehicle cabin, and the battery. After evaporation, the evaporated refrigerant returns to the compressor to continue this cycle.

In addition to this refrigeration cycle, a liquid fluid cooling loop is also active, which is circulated by a pump (6). This loop feeds the coolant into the battery thermal management assembly via path (7). Here, the fluid absorbs the heat generated by the battery, after which the fluid returns to the evaporator to transfer its heat to the refrigerant and re-enter the cooling cycle (5).

The battery configuration in this system is designed as a series–parallel combination; 21 battery packs are connected in series and 6 packs in parallel, each containing 20 cells. This structure is designed to distribute heat evenly and improve thermal safety. This simultaneous interaction between the two cooling loops (refrigerant loop and liquid circuit) significantly improves the thermal performance of the system.

Ultimately, this integrated cooling system ensures that key components of electric vehicles, including the battery, vehicle cabin, electric motor, and inverter, operate at optimal temperature conditions. In Fig. 1, the refrigerant path is shown in green, the coolant path is shown in blue, and the electrical current is shown in red. The working fluids used in this system are water (for the liquid cooling circuit) and HFC type R134a (for the refrigeration cycle).

2.2. Thermodynamic and heat transfer modeling

A systematic methodology was adopted to evaluate the proposed electric vehicle battery cooling system from thermodynamic, exergoeconomic, and exergoenvironmental perspectives. This section outlines the modeling framework, assumptions, and computational tools employed in the analysis. First, the physical configuration of the system and its components is described, followed by the governing energy and exergy equations. Subsequently, the cost and environmental models are introduced to enable the 5E assessment.

2.2.1. Cabin thermal modeling

In electric vehicle air conditioning systems, the cooling load required for the cabin includes the sum of four main heat sources: solar radiation, metabolic heat from the occupants, heat generated by interior electrical equipment, and convective heat transfer from outside air to the cabin. This relationship is expressed as follows [22,27,28]:

$$\dot{Q}_{\text{cab}} = \dot{Q}_{\text{rad}} + \dot{Q}_{\text{human}} + \dot{Q}_{\text{electric}} + \dot{Q}_{\text{con}} \tag{1}$$

Here, $\dot{Q}$ denotes the heat transfer rate. Subscripts cab, rad, human, electric, and con denote the total cabin heat load, the heat gain from solar radiation, the occupants' metabolic heat, the heat from interior electrical devices, and the convective heat transfer from ambient air into the cabin, respectively.

In this work, the solar radiation load was considered only across the window surfaces, as glazing represents the primary pathway for shortwave solar gains in vehicle cabins. Heat absorbed by opaque body panels is comparatively small and is treated indirectly through the convective heat transfer term. This approach is consistent with previous studies [22,27,28] and provides a simplified yet accurate representation of the dominant heat gain mechanisms.

The following relation calculates the solar radiation heating load:

$$\dot{Q}_{\text{rad}} = \Phi_{\text{solar}} \cdot A_{\text{window}} \tag{2}$$

where Φ_{solar} is the intensity of solar radiation and A_{window} is the total surface area of the windows. The internal electrical heat load $\dot{Q}_{\text{electric}}$ is assumed to be constant and equal to 600 W [22,27,28].

To estimate the heat released by human metabolism, the body surface area (BSA) is first calculated using the DuBois empirical formula [29]:

$$\text{BSA} = 0.007184 \cdot W_g^{0.425} \cdot H^{0.725} \tag{3}$$

where W_g is the weight and H is the height of the person. The total metabolic heat gain from passengers is then given by [30]:

$$\dot{Q}_{\text{human}} = \text{BSA} \cdot \left(85 + 55 \cdot (N_{\text{passenger}} - 1)\right) \tag{4}$$

where $N_{\text{passenger}}$ is the total number of occupants. The heat released by each passenger is assumed to be 85 W for the driver and 55 W for each additional passenger.

The convective heat transfer from the ambient environment is calculated using the external convective heat transfer coefficient, which depends on vehicle speed [22,27,28]:

$$h_{\text{external}} = 1.163 \cdot \left(4 + 12 \cdot \sqrt{\frac{V}{3.6}}\right) \tag{5}$$

where V is the vehicle velocity. Accordingly, the convective heat gain through the windows is computed as:

$$\dot{Q}_{\text{con}} = h_{\text{external}} \cdot A_{\text{window}} \cdot (T_{\text{ext}} - T_{\text{cab}}) \tag{6}$$

Table 1
Input parameters used in the cabin thermal load model.

No.	Parameter	Value/Description	Unit
1	Cabin air volume (V_{cab})	2500	liters
2	Inlet air velocity (v_{air})	3	m/s
3	Cabin/system pressure (P_{cab})	100	kPa
4	Cabin temperature (T_{cab})	25	°C
5	External temperature (T_{ext})	35	°C
6	Vehicle velocity (v)	80	km/h
7	Passenger average weight (W)	80	kg
8	Passenger average height (H)	175	cm
9	Number of passengers ($N_{passenger}$)	4	persons
10	Window surface area (A_{window})	2.5	m^2
11	Solar radiation (Φ_{solar})	1000	W/m^2

Here, T_{ext} and T_{cab} are the external and cabin air temperatures, respectively, and A_{window} is the window surface area.

In this study, the convective heat gain was formulated with respect to the window surfaces, as glazing typically has a higher thermal transmittance compared to opaque body panels and therefore dominates the direct convective exchange with the ambient. Heat transfer through the roof, floor, and opaque side walls is implicitly included in the overall thermal balance but is assumed to contribute less significantly than the windows. This simplification, which is also adopted in similar works [22,27,28], provides a tractable model while still capturing the primary pathways of convective heat ingress into the cabin.

Table 1 shows the input parameters for the cabin thermal modeling [22].

2.2.2. Engine thermal modeling

Electric engines in vehicles must overcome rolling resistance, acceleration resistance, and drag (aerodynamic resistance), which determine the mechanical power required, while losses are typically released as heat [22,31], depending on the engine efficiency.

The rolling and acceleration resistance forces, the aerodynamic drag force, and the resulting total resistance force are calculated by the following relations [31]:

$$F_{roll} = f \cdot m_{vehicle} \cdot g \tag{7}$$

$$F_{acc} = \delta \cdot m_{vehicle} \cdot a \tag{8}$$

$$F_{drag} = \frac{1}{2} \cdot C_{drag} \cdot A_{frontal} \cdot \rho_{air} \cdot \left(\frac{v}{3.6}\right)^2 \tag{9}$$

$$F_{total} = F_{roll} + F_{acc} + F_{drag} \tag{10}$$

where, $m_{vehicle}$ is the vehicle mass, g is the gravitational acceleration, δ is the rotating mass correction coefficient, a is the vehicle acceleration, C_{drag} is the aerodynamic drag coefficient, $A_{frontal}$ is the frontal area of the vehicle, ρ_{air} is the air density, and v is the vehicle speed in km/h, converted to m/s by dividing by 3.6. The required mechanical power output of the engine is calculated by the following equation:

$$P_{mot} = \left(\frac{v}{3.6}\right) \cdot F_{total} \tag{11}$$

The final equation calculates the heat loss generated by the engine:

$$\dot{Q}_{mot} = P_{mot} \cdot (1 - \eta_{mot}) \tag{12}$$

where, η_{mot} is the engine efficiency, and the term $(1 - \eta_{mot})$ represents the fraction of power lost as heat. Table 2 shows the input parameters used in the electric engine heat generation model [22,31].

2.2.3. Battery thermal modeling

The thermophysical characteristics of the battery used in this study are presented in Table 3. This battery is a cylindrical lithium-ion battery with a nominal capacity of 2.20 AH and a nominal voltage of 3.70 V. The compact dimensions of this cell and the thermal characteristics of its internal components, including the positive electrode, negative electrode, and separator, make it a suitable option for electric vehicles [32].

Table 2
Input parameters used in the electric engine heat generation model.

No.	Parameter	Value/Description	Unit
1	Rolling resistance coefficient (f)	0.015	–
2	Rotating mass correction coefficient (δ)	1.05	–
3	Vehicle total mass ($m_{vehicle}$)	1500	kg
4	Vehicle acceleration (a)	1	m/s^2
5	Aerodynamic drag coefficient (C_{drag})	0.3	–
6	Vehicle frontal area ($A_{frontal}$)	2.2	m^2
7	Engine efficiency (η_{mot})	0.9	–

Table 3
Geometric and thermophysical characteristics of the selected cylindrical battery cell.

No.	Property	Value	Unit
1	Nominal capacity	2.20	Ah
2	Nominal voltage	3.70	V
3	Cell diameter	18	mm
4	Cell height	65	mm
Positive electrode			
5	Dimensions (L × W × T)	64.5 × 5.8 × 0.144	mm
6	Specific heat capacity	755	J/kg K
7	Thermal conductivity	0.2	W/m K
8	Aluminum foil thickness	0.0164	mm
9	Aluminum foil density	2700	kg/m^3
Negative electrode			
10	Dimensions (L × W × T)	70 × 5.8 × 0.152	mm
11	Specific heat capacity	1437	J/kg K
12	Thermal conductivity	1.1	W/m K
13	Copper foil thickness	0.0107	mm
14	Copper foil density	8930	kg/m^3
Separator			
15	Dimensions (L × W × T)	149 × 6 × 0.020	mm
16	Density	1009	kg/m^3
17	Specific heat capacity	1978	J/kg K
18	Thermal conductivity	0.334	W/m K

To provide the required energy equivalent to 80 kWh at a voltage level of 400 V, the battery cell configuration is designed as a combination of series and parallel arrangements. The cell used is a cylindrical lithium-ion type with a nominal voltage of 3.70 V and a capacity of 2.20 Ampere-hours. Based on these specifications, the number of cells required to achieve the voltage and capacity of the entire system is estimated to be about 9828.

In order to create a modular and deployable structure, the cells are grouped into packages containing 20 cells. Also, considering four parallel paths for the passage of the cooling flow, the number of parallel packages in each path is considered to be equal to 24. In order to maintain the correspondence between the total number of cells and the physical structure of the battery packs, the number of series packages is also rounded to 21. Thus, the entire system will consist of 504 battery packs.

In each cooling path, 24 packages are arranged in parallel, and 21 packages are arranged in series. This structure, in addition to providing the required electrical specifications, allows for uniform heat distribution and an effective cooling system design. The full specifications of this configuration are given in Table 4.

The Bernardi model is one of the simplest and most widely used methods for calculating the heat generated in batteries. This model is based on energy balance and considers the total heat as the sum of reversible heat (due to entropy change) and irreversible heat (Ohmic losses). This equation is expressed as follows [33]:

$$\dot{Q}_{battery} = \frac{I}{V_{bat}} \left(I R_{int} + T \frac{dU_{OC}}{dT} \right) \tag{13}$$

Table 4
Final configuration and key specifications of the electric vehicle battery system for a 400 V, 80 kWh application.

No.	Parameter	Value	Unit
1	Rated voltage per cell	3.70	V
2	Rated capacity per cell	2.20	Ah
3	Total required energy	80,000	Wh
4	System voltage	400	V
5	Number of series cells	108	–
6	Number of parallel cells	91	–
7	Total number of cells	9828	–
8	Cells per package	20	cells
9	Number of parallel packages (rounded)	24	–
10	Number of series packages (rounded)	21	–
11	Total number of packages	504	–
12	Cooling lines (Parallel Flow Paths)	4	–
13	Parallel packages per line	6	–
14	Series packages per line	21	–
15	Total packages per cooling line	126	–
16	Cells per cooling line	2520	cells

Table 5
Mass and energy balance equations for each component of the refrigeration cycle.

No.	Component	Mass conservation equation	Energy conservation equation
1	Compressor	$\dot{m}_1 = \dot{m}_2$	$\dot{W}_{comp} = \dot{m}_1(h_2 - h_1)$
2	Condenser	$\dot{m}_2 = \dot{m}_3$	$\dot{Q}_{cond} = \dot{m}_2(h_2 - h_3)$
3	Expansion valve	$\dot{m}_3 = \dot{m}_4$	$h_3 = h_4$ (Isenthalpic process)
4	Evaporator	$\dot{m}_4 = \dot{m}_1$	$\dot{Q}_{evap} = \dot{m}_4(h_1 - h_4)$

In this equation, I denotes the current, and V_{bat} is the terminal voltage of the cell. R_{int} represents the internal resistance, T is the absolute temperature, and $\frac{dU_{OC}}{dT}$ is the temperature derivative of the open-circuit voltage.

The internal resistance of the battery cell (R_i) and the temperature derivative of the open-circuit voltage ($\frac{dU_{ocv}}{dT}$) are estimated as functions of the state of charge (SOC) shown in the following equations [32]:

$$R_i = 0.0852 + 0.00623 \cdot \sin\left(\frac{\pi \cdot (SOC - 0.23727)}{0.18}\right) \tag{14}$$

$$\begin{aligned}\frac{dU_{ocv}}{dT} &= 3.18467 - 62.78706 \cdot SOC + 425.05006 \cdot SOC^2 \\ &- 1330.74155 \cdot SOC^3 + 2134.38248 \cdot SOC^4 \\ &- 1701.34615 \cdot SOC^5 + 533.88889 \cdot SOC^6\end{aligned} \tag{15}$$

In these equations, R_i represents the internal electrical resistance of the cell varies with the SOC. The term $\frac{dU_{ocv}}{dT}$ denotes the derivative of the open-circuit voltage with respect to temperature. For the base calculation, the SOC and battery set point temperature are considered 0.7 and 35°C, respectively.

2.2.4. Refrigeration cycle modeling

The mass and energy balance equations for the electric vehicle refrigeration cycle are shown in Table 5

In the energy and mass balance equations of the refrigeration cycle, the variable $\dot{m}$ represents the mass flow rate, the symbol h denotes the specific enthalpy, Heat transfer rate is denoted by $\dot{Q}$, while $\dot{W}$ denotes the power input or output. The parameter ε indicates the effectiveness of the internal heat exchange. Subscripts used in the equations include "comp" for the compressor, "cond" for the condenser, and "evap" for the evaporator.

Table 6 shows the input data for the vapor-compression refrigeration cycle.

The required mass flow rate of the refrigeration cycle is calculated from the following equation:

$$\dot{m}_5 = \frac{\dot{Q}_{cab} + \dot{Q}_{battery} + \dot{Q}_{mot}}{h_1 - h_4} \tag{16}$$

Table 6
Input data for the vapor-compression refrigeration cycle.

No.	Parameter	Value	Unit
1	Refrigerant type	R134a	–
2	Evaporator saturation temperature (T_{sat})	5	°C
3	Subcooling degree	3	°C
4	Superheating degree	3	°C
5	Compressor isentropic efficiency (η_s)	0.90	–
6	Condensation temperature (T_{cond})	55	°C
7	Air inlet temperature (Condenser)	25	°C
8	Air outlet temperature (Condenser)	35	°C
9	Air velocity across condenser	18	m/s
10	Fin thermal conductivity (k_{fin})	200	W/m K
11	Fin length (L_{fin})	0.008	m
12	Fin thickness (t_{fin})	0.001	m
13	Added fin area (A_{fins})	1.5	m^2

To account for uncertainties and possible performance fluctuations, these cooling loads are included in the thermal analysis with a confidence factor of 80%.

The coefficient of performance (COP) of the refrigeration cycle is calculated by the following equation:

$$COP = \frac{h_1 - h_4}{h_2 - h_1} \tag{17}$$

2.2.5. Heat transfer analysis

To calculate the required heat exchange area, the logarithmic mean temperature difference (LMTD) equation is used, which is as follows [34]:

$$A = \frac{\dot{Q}}{U \cdot \Delta T_{lm}} \tag{18}$$

$$\Delta T_{lm} = \frac{\Delta T_1 - \Delta T_2}{\ln\left(\frac{\Delta T_1}{\Delta T_2}\right)} \tag{19}$$

In the above equations, A represents the required heat transfer surface area. U is the overall heat transfer coefficient. The term ΔT_{lm} refers to the logarithmic mean temperature difference (LMTD) between the hot and cold streams. ΔT_1 is the temperature difference between the hot stream inlet and the cold stream outlet, while ΔT_2 is the temperature difference between the hot stream outlet and the cold stream inlet. To calculate the convective heat transfer coefficient in single-phase flows, the Nusselt number (Nu) must first be determined. In this study, standard empirical relationships have been used to estimate the Nusselt number, as shown below [34]:

$$Nu = \frac{hD_h}{k} = \begin{cases} 4.36, & \text{if } Re \le 2300 \\ & \text{(Laminar flow, constant heat flux)} \\ \frac{(f_r/8)(Re-1000)Pr}{1+12.7\sqrt{f_r/8}(Pr^{2/3}-1)}, & \text{if } Re > 3000 \\ & \text{(Turbulent flow, Gnielinski)} \end{cases} \tag{20}$$

where h is the convective heat transfer coefficient, D_h is the hydraulic diameter of the channel, k is the thermal conductivity of the working fluid, and f_r represents the Darcy friction factor, which can be determined empirically or through correlations such as the Blasius or Colebrook equations, and is required for the Gnielinski correlation used in turbulent flow conditions.

In two-phase flow thermal design of evaporators and condensers, the Shah correlation is used as shown below [34]:

$$Nu_{tp} = Nu_{lo} \cdot \left[1 + 3.8 \cdot x_{tp}^{0.8} \cdot (1 - x_{tp})^{0.76} \cdot Bo^{0.04} \cdot P_r^{-0.38}\right] \tag{21}$$

$$Bo = \frac{Q_{total}}{G_1 \cdot (h_v - h_l) \cdot A} \tag{22}$$

$$P_r = \frac{P}{P_{\text{crit}}} \tag{23}$$

$$Nu_{\text{lo}} = \frac{h_{\text{sub}} \cdot D_h}{k} \tag{24}$$

In these equations, Bo denotes the boiling number, G_1 denotes the refrigerant mass flux. h_v and h_l represent vapor and liquid enthalpy. The P_r is the reduced pressure. The P_{crit} denotes the critical pressure. Nu_{lo} is the liquid-only Nusselt number. Subscript tp denotes the two-phase flow.

To calculate the Nusselt number on the air side of the condenser, the empirical equation for forced convection of turbulent flow is used [34]

$$Nu = 0.026 \cdot Re^{0.8} \cdot Pr^{0.33} \tag{25}$$

To increase the heat transfer rate on the air side of the compressor, aluminum fins are used. These fins are 1 mm thick and 8 mm long. The efficiency of the fins is calculated for a smooth rectangular geometry by the following equation [34]:

$$m_f = \sqrt{\frac{2h_{\text{air,base}}}{k_{\text{fin}} t_{\text{fin}}}} \tag{26}$$

t_{fin} denotes the fin thickness. The fin efficiency η_f is then calculated by the following equation [34]:

$$\eta_f = \frac{\tanh(m_f L_{\text{fin}})}{m_f L_{\text{fin}}} \tag{27}$$

To determine the overall efficiency of the heat exchange surface, the total surface area with fins is first calculated. The base area (without fins) is equal to [34]:

$$A_b = \frac{A_{\text{cond}}}{\eta_o} - A_{\text{fins}} \tag{28}$$

where A_{fins} is the added area due to the fins, and the total surface area is [34]:

$$A_t = A_b + A_{\text{fins}} \tag{29}$$

The overall surface efficiency η_o, is calculated by [34]:

$$\eta_o = 1 - \left(\frac{A_{\text{fins}}}{A_t}\right)(1 - \eta_f) \tag{30}$$

Finally, the effective convective heat transfer coefficient on the air side is calculated by [34]:

$$h_{\text{air,eff}} = \eta_o \cdot h_{\text{air,base}} \tag{31}$$

2.2.6. Exergy analysis

Specific exergy (e) can be classified into four main categories: physical, chemical, potential, and kinetic exergy [1,35–37].

$$e = \sum x_i e_{\text{ch},i} + \frac{V^2}{2} + gz + (h - h_0) - T_0(s - s_0) + T_0 \sum x_i R_i \ln y_i \tag{32}$$

In this equation, V and z represent the velocity and height of the system, respectively. The parameters x and y represent the mass fraction and mole fraction of each component in the mixture, respectively. Also, s represents the specific entropy. The subscript 0 refers to the reference conditions (or dead state), while the subscripts i and ch are used to specify the chemical components and their chemical exergy, respectively. The exergy destruction rate (EDR) for every system component is shown in Table 7 The total EDR of the refrigerant cycle and total system are calculated by the following equations:

$$\dot{E}_{d,\text{cooling cycle}} = \dot{E}_{d,\text{comp}} + \dot{E}_{d,\text{cond}} + \dot{E}_{d,\text{exp.valve}} + \dot{E}_{d,\text{evap}} \tag{33}$$

$$\dot{E}_{d,\text{system}} = \dot{E}_{d,\text{comp}} + \dot{E}_{d,\text{cond}} + \dot{E}_{d,\text{exp.valve}} + \dot{E}_{d,\text{evap}} + \dot{E}_{d,\text{cab}} + \dot{E}_{d,\text{BCP}} + \dot{E}_{d,\text{engine}} \tag{34}$$

Table 7
Exergy destruction rate (EDR) expressions for individual system components.

No.	Component	Exergy destruction expression (kW)
1	Compressor	$\dot{m}_1(e_1 - e_2) + \dot{W}_{\text{comp}}$
2	Condenser	$\dot{m}_2(e_2 - e_3) + \dot{m}_{\text{air,cond}}(e_{\text{air,in,cond}} - e_{\text{air,out,cond}})$
3	Expansion valve	$\dot{m}_4(e_3 - e_4)$
4	Cabin	$\dot{Q}_{\text{cab}} \cdot \left(1 - \frac{T_0}{T_{\text{cab}}+273.15}\right)$
5	Battery cooling path (BCP)	$\dot{m}_5(e_7 - e_5)$
6	Engine	$\dot{Q}_{\text{mot}} \cdot \left(1 - \frac{T_0}{T_{\text{mot}}+273.15}\right)$
7	Evaporator	$(\dot{E}_{d,\text{cab}} + \dot{E}_{d,\text{battery}} + \dot{E}_{d,\text{engine}}) - \dot{m}_4(e_1 - e_4)$

The refrigerant cycle exergy efficiency is calculated by the following relation:

$$\eta_{\text{ex}} = \frac{\dot{m}_5(e_1 - e_4)}{\dot{W}_{\text{comp}}} \tag{35}$$

2.2.7. Exergo-environmental analysis

Exergy-environmental analysis combines the concepts of exergy analysis and environmental impact assessment to measure the side effects of EDR in energy systems. This approach examines how inefficiencies in real-world processes lead to depletion of natural resources and environmental damage. To measure the relationship between EDR and its environmental impacts, an index named the exergy-environmental factor is defined, which can be calculated by the following equation [36,38,39]:

$$f_{ei} = \frac{\text{EDR}}{\sum_{\text{in}} \dot{m}e} \tag{36}$$

The system's Environmental Damage Effectiveness Ratio (EDE) is defined to measure the impact of the EDR on the environment. This parameter can be calculated by the following equation [36,38,39]:

$$\phi_{ei} = \frac{f_{ei}}{\eta_{ex}} \tag{37}$$

The Exergy Stability Factor (ESF) evaluates the balance between the EDR and the exergy Output rate. This index can be calculated by the following equation [36,38,39]:

$$f_{es} = \frac{\text{EDR}}{\sum \dot{m}e_{\text{xtot,out}} + \text{EDR} + 1} \tag{38}$$

2.3. Economic analysis

Table 8 shows the cost functions for every component of the proposed system. O&M (operating and maintenance) costs are assumed to be 6% of the initial

The isentropic efficiency of the compressor is denoted by η_s. C_{pump} denotes the corresponding cost exponent, varying with power level. The term $\dot{m}_{\text{ref,a}}$ indicates the refrigerant mass flow rate through the expansion valve. C_{bat}, is the cost per unit of battery energy capacity in USD/kWh, and K_{bat} specifies the amount of battery energy (in kWh). The total investment cost of the proposed system can be determined by the following equation [47–49]:

$$Z_0 = Z_{\text{comp}} + Z_{\text{cond}} + Z_{\text{evap}} + Z_{\text{pump}} + Z_{\text{EXV}} + Z_{\text{bat}} + Z_{\text{channel}} \tag{39}$$

where Z denotes the investment cost of each subsystem.

The impact of the inflation rate can be considered by using the following relation [50]:

$$Z_n = Z_0(1 + i)^n \tag{40}$$

Here, i denotes the inflation rate (equal to 2.5%) and n denotes the number of years of operation.

The capital recovery factor (CRF) is calculated by the following relation [50]:

$$\text{CRF} = \frac{i(1 + i)^n}{(1 + i)^n - 1} \tag{41}$$

Table 8
Cost functions used for the economic modeling of system components.

No.	Component	Cost equation	Ref
1	Compressor	$Z_{comp} = \left(\frac{573\,\dot{m}_{ref}}{0.8996-\eta_s}\right)\left(\frac{P_{cond}}{P_{evap}}\right)\ln\left(\frac{P_{cond}}{P_{evap}}\right)$ $\eta_s = 0.85 - 0.046667\left(\frac{P_{cond}}{P_{evap}}\right)$	[40]
2	Condenser	$Z_{cond} = 516.621\,A_{cond}$	[41]
3	Evaporator	$Z_{evap} = 309.143\,A_{evap}$	[41]
4	Pump	$Z_{pump} = 308.9\,\dot{W}_{pump}^{C_{pump}}$ $C_{pump} = 0.25$ for $0.02 < \dot{W}_{pump} < 0.3$ kW $C_{pump} = 0.45$ for $0.3 < \dot{W}_{pump} < 20$ kW $C_{pump} = 0.84$ for $20 < \dot{W}_{pump} < 200$ kW	[41]
5	Expansion valve (EXV)	$Z_{evap,exv} = 5000\,\dot{m}_{ref,a}$	[42]
6	Battery cooling channel	$Z_{channel} = 250\,A_{bat,channel}$	[43–46]
7	Battery pack (for TMS)	$Z_{bat} = C_{bat}K_{bat}$	[41]

i denotes the annual interest rate (8%) in this article, and n is the equipment lifetime (10 years in this study).

The marginal cost of cooling produced by an electric vehicle refrigeration system is calculated using the following equation.

$$C_{cooling} = \frac{Z_n}{E_{cooling,\ annual}} \tag{42}$$

$E_{cooling,\ annual}$ represents the total cooling energy produced by the refrigeration system during 3000 h of operation in one year.

2.4. Exergoeconomic analysis

Exergoeconomic analysis provides a more detailed view of the performance of energy systems by incorporating economic concepts into exergy analysis. This method calculates the cost of exergy flows in the system and determines the final cost of the product of each component. It also identifies the relationship between the costs of flows and the investment in different components of the system. For each component of the system, a cost balance is considered that includes the flows' costs and the investment cost of that component [51–53].

In this regard, the Specific Exergy Costing (SPECO) methodology was adopted to assign monetary values to the exergy streams of the system. This approach establishes cost balances for each component by linking the unit cost of exergy at the inlet and outlet streams with the cost of capital investment and operating expenses. Through this procedure, the cost of exergy destruction and losses is quantified, allowing identification of the components with the highest economic impact [51–53].

The general equation of exergoeconomic analysis is as follows [51–53]:

$$\dot{C}_{q,k} + \sum_i \dot{C}_{i,k} + \dot{Z}_k = \sum_e \dot{C}_{e,k} + \dot{C}_{w,k} \tag{43a}$$

$$\dot{C}_i = c_i\,\dot{E}_i = c_i\,\dot{m}_i\,e_i \tag{43b}$$

$$\dot{C}_e = c_e\,\dot{E}_e = c_e\,\dot{m}_e\,e_e \tag{43c}$$

$$\dot{C}_w = c_w\,\dot{W} \tag{43d}$$

$$\dot{C}_q = c_q\,\dot{E}_q \tag{43e}$$

The term $\dot{C}$ represents the cost rate; Subscripts i, e, q, and w denote input, outlet, thermal, and work. The term $\dot{Z}_k$ denotes the capital investment and maintenance cost rate attributed to the component. k denotes the number of components. c is the unit exergy cost. $\dot{E}$ is the exergy flow rate.

The cost rate of the EDR is defined as follows:

$$\dot{C}_{D,k} = c_{F,k}\,\dot{E}_{d,k} \tag{44}$$

Table 9
Exergoeconomic cost balance equations for system components.

No.	Component	Equation
1	Compressor	$\dot{C}_1 + \dot{Z}_{comp} + c_{elect}\cdot\dot{W}_C = \dot{C}_2$
2	Condenser	$\dot{C}_2 + \dot{C}_{air,in,cond} + \dot{Z}_{cond} = \dot{C}_3 + \dot{C}_{air,out,cond}$
3	Expansion valve (EXV)	$\dot{C}_3 + \dot{Z}_{EXV} = \dot{C}_4$
4	Evaporator	$\dot{C}_4 + \dot{Z}_{evap} + c_{cool}\cdot\dot{Q}_{total} = \dot{C}_1$
5	Battery cooling channel	$\dot{C}_5 + \dot{Z}_{channel} = \dot{C}_7$
6	Coolant pump	$\dot{C}_5 + \dot{Z}_{pump} + c_{elect}\cdot 5\cdot\dot{W}_{pump} = \dot{C}_6$
7	Battery channel – F-rule	$\dot{C}_5\cdot\dot{m}_7\cdot e_7 = \dot{C}_7\cdot\dot{m}_5\cdot e_5$
8	Compressor – F-rule	$\dot{C}_1\cdot\dot{m}_2\cdot e_2 = \dot{C}_2\cdot\dot{m}_1\cdot e_1$
9	Assumption	$\dot{C}_{air,in,cond} = 0$

The capital investment rate can be calculated by the following equation:

$$\dot{Z}_k = \frac{Z_k\cdot CRF\cdot\varphi}{N} \tag{45}$$

where N is the unit's annual number of operation hours and φ is the maintenance factor. The total cost rate is calculated as follows:

$$\dot{C}_{tot,k} = \dot{C}_{D,k} + \dot{Z}_k \tag{46}$$

Ultimately, the exergoeconomic factor is given by the following relation:

$$f_k = \frac{\dot{Z}_k}{\dot{Z}_k + c_{f,k}\,\dot{E}_{D,k}} \tag{47}$$

Table 9 shows the exergoeconomic relations for each component plus the F-rule auxiliary equation

2.5. Mathematical modeling implementation

The mathematical model presented in the previous sections is developed in the *Engineering Equation Solver (EES)* software. All properties required for system performance simulation are extracted directly from the EES property database. The boundary conditions and operating parameters used in the simulations (ambient temperature, pressure levels, mass flow rates, component efficiencies, and heat transfer coefficients) are summarized in Tables 1, 2, 3, 4, and 6, respectively.

To validate the numerical model and also to check the accuracy and consistency of the results, a similar computational code is also developed completely in *Python*. In this version of the model, thermodynamic and physical property calculations have been done using *CoolProp* library. CoolProp is an open-source library for thermodynamic properties.

The purpose of developing the model in both EES and Python is to examine the consistency of the numerical results, identify possible differences in the calculation of thermodynamic properties between the two databases, and evaluate the performance of the equation-solving algorithms in each software. This comparison helps to increase

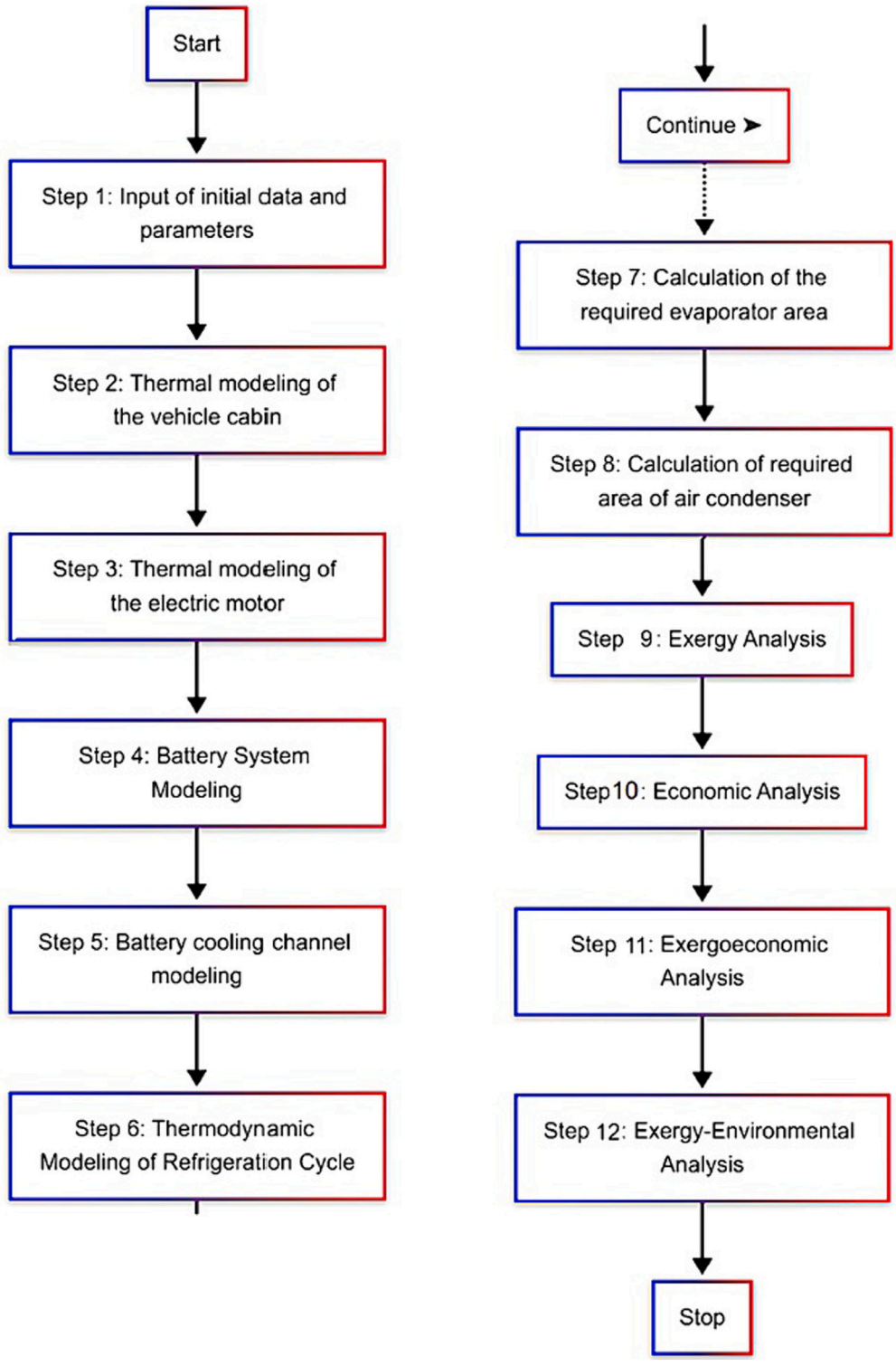

Fig. 2. Flowchart illustrating the calculation procedure of the proposed model.

confidence in the accuracy of the results and the stability of the model. The procedure adopted by the simulation model is based on the steps described in Fig. 2.

3. Result and discussion

This section presents and discusses the main findings of the thermodynamic, exergo-economic, and exergo-environmental analyses of the proposed electric vehicle battery cooling system. The results are structured to highlight the system's energy and exergy performance, followed by a detailed cost and environmental assessment. Comparisons with conventional configurations are provided to demonstrate the advantages of the proposed layout. Sensitivity analyses are also included to evaluate the influence of key design and operating parameters. Together, these results provide a comprehensive understanding of the system's technical, economic, and environmental feasibility.

Table 10
Validation of the proposed model through comparison of simulation and experimental results.

No.	Parameter	Unit	Experimental	Simulation	Relative error (%)
1	Evaporator capacity	kW	4.25	4.40	3.53
2	Condenser capacity	kW	5.85	5.97	2.05
3	Compressor power	kW	1.60	1.55	3.13
4	COP	–	2.66	2.83	6.39

3.1. Model validation

A structured validation procedure was performed for all sub-models of the proposed thermal management system, including the cabin, motor, battery, and refrigeration cycle models.

Experimental data from field tests performed at the Guangzhou Higher Education Center [22,27] were used to validate the cabin thermal model. The comparison between measured and simulated cabin temperatures showed a maximum absolute deviation of 3.53°C and a relative error below 5%. In addition, the conductive thermal load measured using an HFM-215 heat flux meter was approximately 900 W, in good agreement with model predictions. Statistical indicators confirmed the robustness and reliability of the cabin model.

The motor heat generation model was validated using data reported in [22,31]. In the reference study, a 42.9 kW electric motor with an efficiency of 42.9% produced approximately 40 kW of thermal losses with a heating efficiency of 70%. Comparison with the present model demonstrates an error margin of less than 3%, confirming the accuracy of the thermal formulation.

The internal resistance and thermal entropy coefficient of the battery were computed using empirical relationships from [32]. The original data-fitting process reported coefficients of determination of $R^2 = 0.82$ for internal resistance and $R^2 = 0.97$ for thermal entropy. These high determination coefficients confirm the suitability of the correlations for battery thermal modeling.

The refrigeration cycle model was validated using experimental measurements from [54]. The same inlet conditions as the laboratory tests were applied to the numerical model, and key parameters, including evaporator and condenser capacity, compressor power, and COP were compared.

The results of the validation process is reported in Table 10 where it can be observed that the models are in agreement with the results from the literature, since all relative errors remaining within acceptable engineering limits.

3.2. Energy and exergy analysis results

Table 11 shows the physical properties at various points of the system. The table shows data on mass flow rates, pressure, temperature, specific enthalpy, entropy, and exergy. Table 12 presents the key values of thermal loads, power consumption, and performance indicators of the proposed refrigeration cycle. The cabin cooling load is 3.83 kW, which is calculated from the sum of the effects of solar radiation, heat generated by the occupants, electrical equipment, and engine heat losses, and is consistent with the reference values for summer weather conditions. The engine thermal power (4.4 kW) and solar radiation (2.5 kW) are also consistent with the experimental values of electrical losses and ambient radiation conditions, confirming the accuracy of the thermal model. The evaporator cooling capacity and condenser heat capacity are 16.1 and 20.2 kW, respectively. The compressor power consumption is also 4.2 kW, resulting in a coefficient of performance (COP) of 3.81. This value is within the appropriate performance range for electric vehicle cooling systems and indicates favorable energy efficiency. Also, the thermal load of the battery is estimated to be 7.8 kW, which is consistent with the actual operating conditions of batteries in electric vehicles.

Table 11
Physical properties at each point of the revised system configuration.

No.	Fluid	$\dot{m}$ (kg/s)	P (kPa)	T (°C)	h (kJ/kg)	s (kJ/kg K)	e (kJ/kg)
1	R134a	0.1235	349.9	8.00	256.1	0.9386	2.943
2	R134a	0.1235	1492	65.55	290.1	0.9487	34.20
3	R134a	0.1235	1492	52.00	126.5	0.4508	7.126
4	R134a	0.1235	349.9	5.00	126.5	0.4729	1.057
5	Water	0.1858	100	25.00	104.9	0.3672	4.157
6	Water	0.1858	100	25.00	104.9	0.3672	4.157
7	Water	0.1858	100	15.00	63.08	0.2244	1.449

Table 12
Summary of thermal and performance parameters.

No.	Parameter	Symbol	Value	Unit
1	Cabin cooling load	$\dot{Q}_{cab}$	3.83	kW
2	Electric component heat load	$\dot{Q}_{electric}$	0.60	kW
3	Human body heat load	$\dot{Q}_{human}$	0.49	kW
4	Engine heat load	$\dot{Q}_{mot}$	4.40	kW
5	Radiation load	$\dot{Q}_{rad}$	2.50	kW
6	Total condenser heat rejection	$\dot{Q}_{cond}$	20.2	kW
7	Total evaporator heat absorption	$\dot{Q}_{eva}$	16.1	kW
8	Compressor power input	$\dot{W}_C$	4.2	kW
9	Battery thermal load	$\dot{Q}_{Battery}$	7.8	kW
10	Total thermal load	$\dot{Q}_{Total}$	16	kW
11	Coefficient of performance	COP	3.81	–
12	Exergy efficiency	η_{ex}	5.5	%

The calculated value for the exergy efficiency of the entire system is 5.5%. This value, compared to the COP of 3.81, clearly shows that although the COP value of 3.81 confirms that the system provides an acceptable energy performance, the exergy efficiency of only 5.5% highlights a substantial gap between energy quantity and energy quality. The low exergy efficiency of the system (5.5%) is fundamentally linked to the nature of the battery thermal management cycle, whose main components operate under highly irreversible conditions. The evaporator and battery cooling heat exchanger impose large temperature differences between the refrigerant and the thermal load, generating significant entropy during heat transfer. Another major contributor is the compressor, where non-ideal compression, mechanical friction, and pressure drops increase the entropy generation and reduce the available exergy of the refrigerant. The throttling valve is also inherently highly irreversible due to its isenthalpic expansion process, leading to additional exergy losses. Finally, the thermal level mismatch between the battery (about 30–40°C) and the evaporating refrigerant temperature (about −5 to 5°C) forces the cycle to operate across large ΔT values, which further intensifies irreversibility. These combined factors, rather than simple overall system inefficiency, are the underlying reasons for the low exergy efficiency.

These results highlight an important point in the design of thermal management systems for electric vehicles: components that perform reasonably well in terms of COP may still contribute significantly to exergy degradation. Therefore, using COP alone cannot provide an accurate picture of the true efficiency of the cycle and may lead to incorrect design decisions. Furthermore, the findings show that even relatively small reductions in the heat exchanger temperature difference or in compressor loading can lead to significant improvements in exergy efficiency. This highlights the importance of considering energy quality-based criteria and provides a clear path to increasing system efficiency by reducing irreversibilities, improving heat exchanger design, and optimizing operating conditions.

Fig. 3 shows the percentage distribution of the EDR in each component of the cooling system.

Fig. 3 indicates that the evaporator exhibits the highest share of EDR, accounting for nearly half of the destruction. This dominance

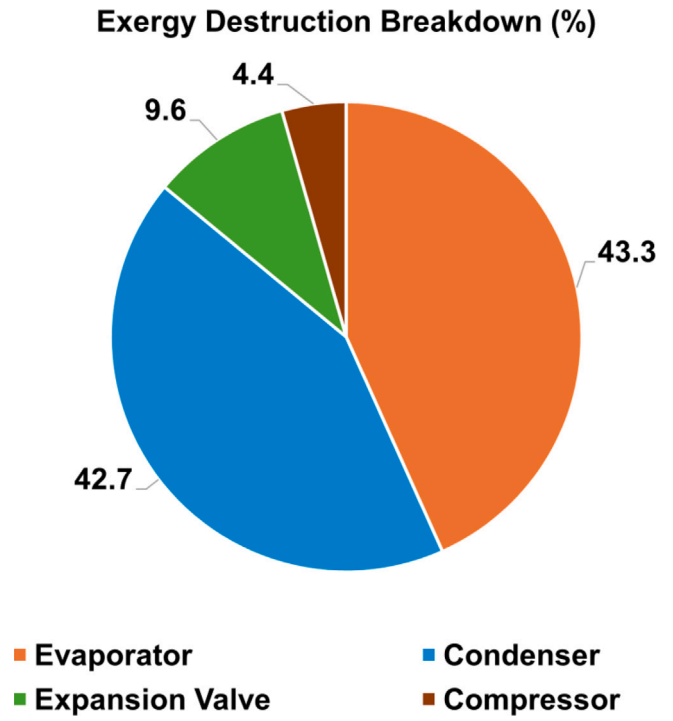

Fig. 3. Percentage distribution of the EDR in each component of the cooling system.

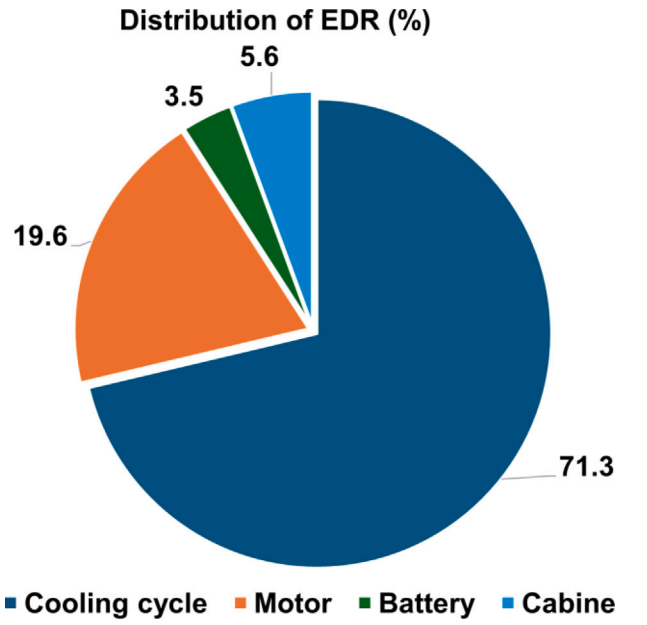

Fig. 4. Percentage distribution of the EDR in each subsystem.

arises from its operating conditions – low pressure, low temperature, and large thermal load from the battery, motor, and cabin – which intensify thermodynamic irreversibilities. The condenser also shows a considerable contribution due to the large temperature difference between the refrigerant and ambient air. In contrast, the compressor and expansion valve contribute marginally, confirming that most irreversibilities originate from the heat exchangers rather than mechanical components.

Identifying the evaporator and condenser as the dominant sources of EDR highlights their priority for system optimization. Improving heat exchanger design — such as, increasing heat transfer area, reducing pressure drop, and optimizing flow distribution – can significantly reduce thermodynamic losses. Refrigerant selection also plays an important role, as fluids with more favorable thermophysical properties can reduce the temperature lift and compressor work. Finally, system-level improvements can be achieved through optimized operating conditions (flow rates, pressures, and temperatures) and the use of advanced control strategies capable of adapting performance to varying loads. These measures collectively provide a clear pathway for reducing exergy destruction and improving the overall efficiency of EV cooling systems.

These results provide an important insight into the thermodynamic behavior of electric vehicle cooling systems: a large part of the irreversibility is not due to mechanical components, but rather to the temperature difference required to exchange heat with the environment. Therefore, improving system performance is not achieved by increasing the efficiency of the components alone, but rather by focusing on reducing the temperature difference of the heat exchangers and better managing the heat transfer conditions. The dominance of EDR in the evaporator and condenser indicates that the design of future generations of electric vehicle thermal systems should prioritize reducing the temperature mismatch under variable load conditions, as this has a direct impact on the vehicle's driving range, battery degradation, and overall system energy consumption. This exergy-based analysis not only identifies the location and severity of losses, but also outlines new priorities for the design of future thermal management systems.

Fig. 4 shows the percentage distribution of the EDR in each subsystem. The cooling cycle has the largest share of EDR. This is due to the large number of active components in the cooling cycle and the presence of phase change processes.

The electric engine is the second-highest EDR in the system due to electrical losses, mechanical friction, and heat generation. The EDR in the cabin and battery subsystems is relatively lower, which could indicate better performance of these subsystems.

In general, this graph shows that the greatest potential for improving the exergy efficiency of the system lies in optimizing the components of the cooling cycle and reducing the heat losses in the engine. Focusing on improving the design of heat exchangers, using refrigerants with better thermodynamic performance, and optimizing the performance of the compressor and evaporator can lead to a significant reduction in the EDR of the entire system.

In the case of electric engines, the reduction of EDR can be achieved through a set of targeted measures. One of the most important solutions is to reduce mechanical friction in the moving parts of the engine, which is possible by optimizing the design of bearings, using lubricants with appropriate thermophysical properties, and reducing unnecessary backlash.

In addition, improving the thermal and electrical properties of the insulating materials used in the windings and engine core, such as using composite materials with appropriate thermal conductivity and high dielectric strength, can reduce losses due to ohmic heating and hysteresis, and thus limit the amount of thermal irreversibility.

In addition, the implementation of intelligent and responsive thermal control systems is also of great importance. Such systems, using temperature sensors and advanced control algorithms, are able to adjust the operating conditions of the engine in real time and prevent the occurrence of high temperatures or performance fluctuations that cause a drop in exergy efficiency. These integrated approaches are not only effective in optimizing engine performance but also will make a significant contribution to reducing the EDR of the entire thermal system of electric vehicles.

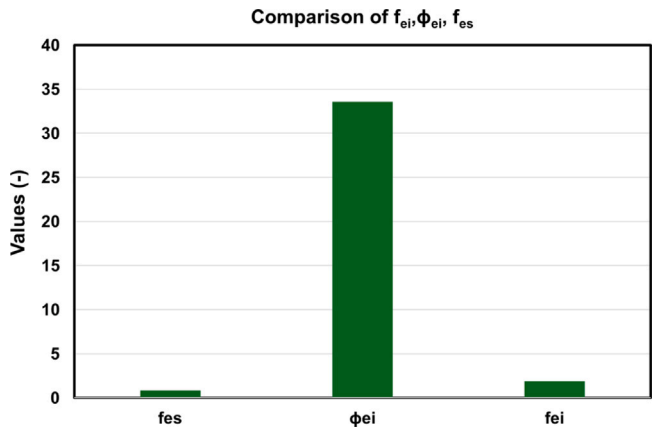

Fig. 5. Comparison of f_{ei}, φ_{ei}, and f_{es} for the electric vehicle refrigeration cycle.

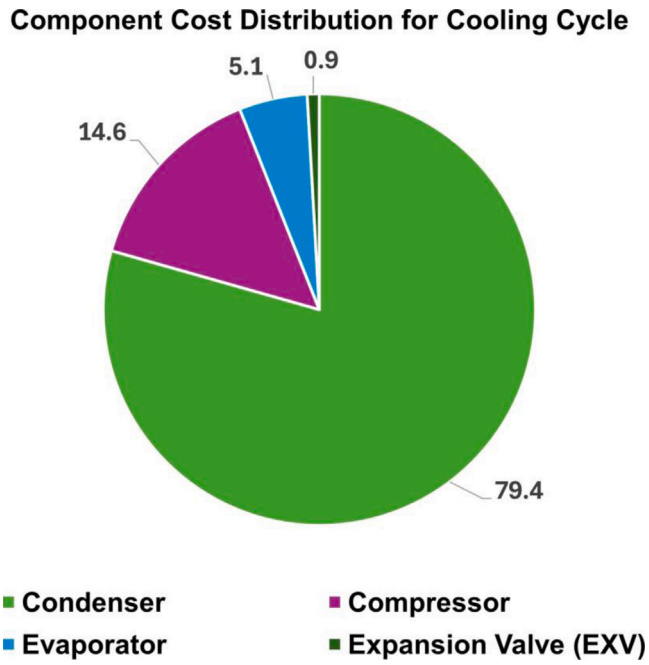

Fig. 6. Cost breakdown of the main components in the cooling cycle.

3.3. Exergo-environmental analysis results

Fig. 5 examines three key indicators in exergy-environmental analysis. The relatively high value of f_{ei} indicates that the EDR is significant compared to the inlet exergy rate. This clarifies that a considerable part of the inlet exergy rate is lost because of the irreversibility of the processes that are not converted into useful work or effective exergy output. In fact, the higher the value of f_{ei}, the greater the share of EDR relative to the energy input, indicating lower efficiency and more environmental impacts due to irreversibility. A high value of φ_{ei} indicates that the EDR in the system is very high compared to the exergy efficiency. From a thermodynamic point of view, this indicates an unbalanced operation of the system and the presence of irreversible processes. In such conditions, a significant part of the input exergy is lost without being converted into useful work or cooling, which leads to a decrease in exergy efficiency and an increase in the depletion of energy resources and the environment. Finally, a high value of f_{es} indicates that the contribution of exergy destruction to the useful exergy output is high, which indicates low thermodynamic performance and inefficient utilization of energy resources. This state leads to increased consumption of primary resources and increased negative environmental impacts.

The high values of f_{ei}, φ_{ei}, and f_{es} in this system indicate that a major part of the environmental impacts is caused by processes that occur with large temperature differences in the heat exchangers. In other words, the largest contribution of exergy destruction, and consequently the largest environmental impacts, does not come from mechanical components such as the compressor, but from the evaporator and condenser, where the highest thermodynamic imbalance occurs. This indicates that to reduce the environmental impacts of the cycle, the focus should be on reducing temperature lift, improving the design of the exchangers, and selecting refrigerants with appropriate thermodynamic performance. This analysis also highlights that increasing exergy efficiency is not only a technical goal but also an environmental imperative, as reducing exergy degradation directly leads to lower primary resource consumption and reduced environmental impacts. Such insight provides a clear path for designing more sustainable thermal management systems for electric vehicles.

3.4. Economic analysis results

Fig. 6 shows the cost distribution of the main components of the refrigeration cycle. As can be seen, the condenser accounts for the highest cost with a share of 79.4%, followed by the compressor and evaporator with 14.6% and 5.1%, respectively. EXV has a very small share of the total system cost. The high share of the condenser in the total cost is mainly due to the need for large heat transfer surfaces for cooling the working fluid of the cycle. These results indicate that economic and thermodynamic optimization of the refrigeration cycle should be focused specifically on improving the performance and reducing the costs of the condenser and compressor, because improvements or changes in components with a low cost share will not have a significant impact on reducing the total cost of the system. So, the development of new technologies in the design of condensers, increasing the efficiency of compressors, optimizing heat transfer processes, and using advanced materials can play an effective role in improving the overall cycle efficiency and enhancing the economic aspects of refrigeration systems.

Based on the calculations performed in the economic model, the cost of cooling produced by the electric vehicle cooling system is obtained as 0.055 US$/kWh. In these calculations, 3000 annual operating hours, an inflation rate of 2.5%, an annual interest rate of 8%, and a life time of the equipment equal to 10 years are considered. From a thermodynamic engineering perspective, the cost of cooling depends on the performance and efficiency of the main components of the system, including the compressor, condenser, evaporator, and cooling channels. Improving the efficiency of these components can reduce energy consumption and, as a result, improve the cost of cooling.

3.5. Exergo-economic analysis results

Table 13 presents the values of the cost rate ($\dot{C}$) and the specific exergy cost (c) for various system components, which are used in the exergoeconomic analysis to calculate the cost of exergy flows and the economic evaluation of the components.

According to the results, the highest exergy cost rate is associated with the condenser, with a value of $\dot{C}$ = 13.82 (US$/s). This high value indicates that the condenser contributes the most to the exergoeconomic cost of the system. The reason for this is the significant heat exchange with the ambient air and the reduction in energy quality during the condensation process. The compressor also has a considerable cost share, with $\dot{C}$ = 1.189 (US$/s), which is due to its direct

Table 13
Calculated values of cost rate ($\dot{C}$) and unit cost (c) for system components.

No.	$\dot{C}$	c
1	1.189	3.271
2	13.82	3.271
3	0.2991	0.3399
4	0.3004	2.302
5	0.01385	0.05144
6	0.0762	0.2831
7	0.03972	0.05144

consumption of electrical energy to compress the refrigerant. Its specific exergy cost ($c = 3.271 US\$$) is also relatively high, indicating the high quality of the energy input.

Although a large pressure drop occurs in the expansion valve, its exergy cost is relatively low. This is because it does not directly consume any energy, but the EDR resulting from the isenthalpic expansion process leads to a cost rate of $\dot{C} = 0.2991$ (US$/s). For the evaporator, the specific cost value ($c = 2.302 US\$$) is relatively high, which reflects the thermal importance of this component in absorbing heat from the battery and vehicle cabin.

In the battery cooling section, components such as the cooling channel and its outlet show very low cost rates, calculated as $\dot{C} = 0.01385$ (US$/s) and $\dot{C} = 0.03972$ (US$/s), respectively. This indicates that the battery cooling subsystem does not impose a significant economic burden on the system. The coolant pump, with $\dot{C} = 0.0762$ (US$/s) and a relatively low specific cost, plays a low-cost role in circulating the coolant.

Overall, the results show that in addition to key components such as the compressor and condenser, which impose high economic costs on the system, components like the pump and cooling channels have a lower economic impact. This information can be utilized to optimize system design and reduce investment and operational costs.

Fig. 7 shows the cost rate of exergy destruction ($\dot{C}_D$) for the main components of the electric vehicle cooling system. According to these results, the largest contribution to the cost of exergy destruction is related to the condenser. This section causes the largest energy quality losses due to the intense heat exchange with the ambient air in the condensation process. From a physical point of view, these losses are due to entropy generation and heat rejection at a lower temperature level to the environment. From an engineering point of view, the use of optimal heat exchange surfaces or improved airflow design can help reduce this destruction.

On the other hand, the evaporator is responsible for absorbing heat from the battery, vehicle cabin, and motor, and experiences significant exergy destruction due to the high temperature difference between the cooled fluid and the refrigerant. Non-ideal processes, such as incomplete heat transfer or pressure drop in the flow path, can also increase this cost. Optimization of temperature distribution, better design of internal surfaces, and flow control are some of the solutions to reduce these losses. Further in-depth analyses taking account different evaporator configurations would allow to understand deeply the influence of the main design technical parameter on the exergy destruction of the investigated system.

The compressor has a moderate contribution to the cost of exergy destruction. In this section, high-quality electrical energy enters the system, and the compression process increases the temperature and pressure of the refrigerant. Exergy losses in this component are mainly due to non-ideal thermodynamic processes and mechanical friction. Improving isentropic efficiency and choosing a more appropriate compressor type can reduce losses in this section.

Finally, the expansion valve has the least contribution to the cost of exergy destruction. Although this component does not consume energy, the isenthalpic process creates a severe pressure drop that leads to the destruction of part of the exergy. The use of internal heat exchangers or alternative designs can reduce this type of loss.

These results show that the bulk of the cost of EDR in the system is concentrated in the heat exchangers, not in the mechanical components. This shifts the design priority from improving compressor performance to reducing the temperature difference and irreversibilities in the condenser–evaporator pair. From a systems engineering perspective, this means that even small improvements in heat exchanger efficiency, better refrigerant selection, or better airflow management can significantly reduce the overall cooling cost. Thus, exergo-economic assessment not only quantifies the current losses but also provides a clear path for economic optimization and design of the next generation of thermal management systems for electric vehicles.

Fig. 8 shows the exergo-economic factors of the components of the electric vehicle cooling system. Low values of this factor in different components of the cooling system indicate that the share of costs due to the EDR is dominant compared to the investment and maintenance costs of the components. In other words, the largest part of the costs associated with each component is due to thermodynamic inefficiencies.

From an exergo-economic perspective, this situation indicates that focusing solely on reducing investment costs without improving the thermodynamic efficiency of components cannot effectively reduce the costs of the entire system. Therefore, optimizing the design of components with the greatest EDR can significantly contribute to reducing the total system cost.

3.6. Parametric analysis results

Fig. 9 shows the effect of the SOC on the cooling cost and the total cost rate. These two values are decreased with SOC from 0.2 to about 0.7. This trend is due to reduced heat generated in the battery and improved energy efficiency. The minimum point is observed at about SOC = 0.7, indicating the optimal conditions from a thermodynamic and economic perspective for the operation of the cooling system. After passing approximately SOC ≈ 0.7, due to the gradual increase in internal resistance and also the growth of the derivative of the open-circuit voltage by temperature, the amount of heat returned to the system increases, and consequently, the cooling cost and the total cost rate increase.

In general, the economic and exergoeconomic performance of the battery cooling system is optimum in the mid-SOC ranges (particularly between 0.65 and 0.75), and designing thermal management strategies within this range can lead to improved energy sustainability and reduced operating costs.

Fig. 10 shows the effect of changing the dead state temperature (T_0) on the exergy efficiency and the EDR of the system. As can be seen, both indices tend to decrease as the reference temperature increases from 1 to 5 degrees Celsius.

Exergy efficiency (η_{ex}) is strongly dependent on the difference between the operating temperature of the system components and the dead state temperature. As T_0 increases, the temperature difference between the components (such as the evaporator and condenser) and the environment decreases, and as a result, the potential for doing useful work decreases. In other words, a larger part of the input energy remains in the system as heat loss, and the ability to be converted into useful work is lost. This is the main reason for the sharp decrease in exergy efficiency with increasing T_0.

These results show that increasing the reference dead temperature has a dual effect: on the one hand, it drastically reduces the exergy efficiency, because the potential for useful work production becomes smaller; and on the other hand, the EDR apparently decreases, because the difference between the actual and reference conditions is considered smaller. Therefore, the choice of reference temperature in exergy analyses plays a very decisive role and should be chosen carefully based on physical and practical considerations.

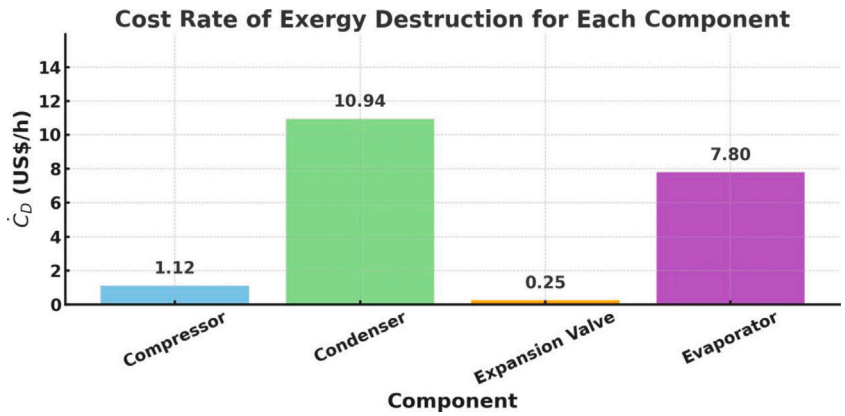

Fig. 7. Cost rate of exergy destruction for each component in the cooling system.

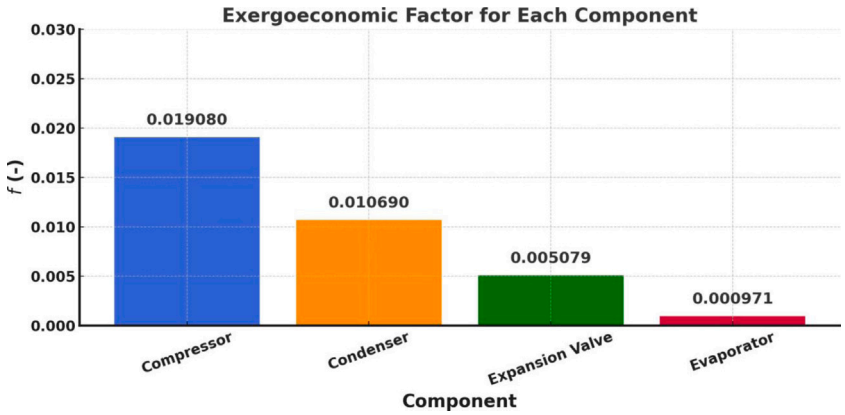

Fig. 8. Exergo-economic factor for the main components of the electric vehicle cooling system.

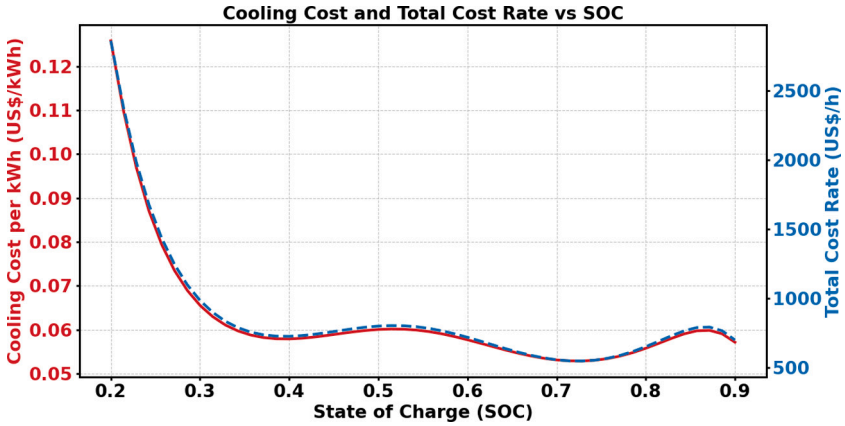

Fig. 9. Effect of the battery state of charge (SOC) on the cooling cost and total cost rate of the electric vehicle cooling system.

Fig. 11 shows the changes in the total cost rate of the electric vehicle cooling system against the difference in ΔT_E. As is clear from the graph, with a gradual increase in ΔT_E from 2 to 18 degrees Celsius, the total cost rate of the system also increases uniformly and upward. This trend indicates that an increase in the operating temperature difference in the system components, especially in the evaporator and condenser, leads to an increase in investment and operating costs.

At the same time, in accordance with the results obtained from the previous figure, an increase in ΔT_E leads to an improvement in the thermodynamic performance of the cooling system; in such a way

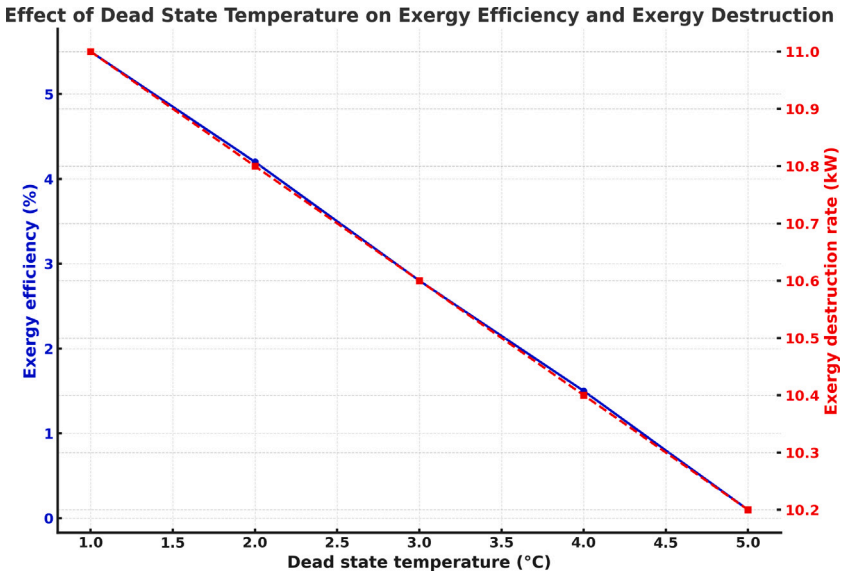

Fig. 10. Comparison of exergy efficiency and exergy destruction rate of the electric vehicle cooling system under varying dead state temperature (T_0).

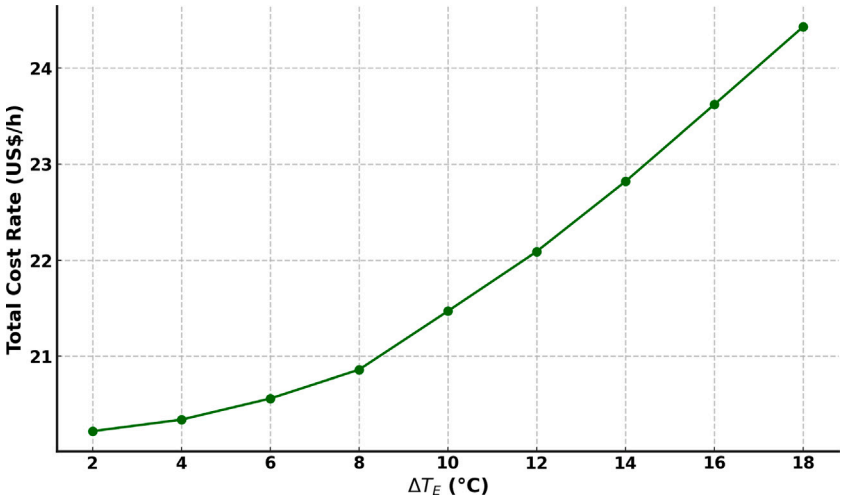

Fig. 11. Variation of total cost rate of the electric vehicle cooling system concerning ΔT_E.

that both the coefficient of performance (COP) and exergy efficiency show an upward trend with an increase in ΔT_E. This is because a larger temperature difference provides more favorable conditions for heat exchange, increases the useful heat transfer rate, and reduces the entropy generation in the system.

However, an inverse relationship is observed between improving thermodynamic indices and increasing costs. In other words, although the system performance improves in terms of energy and exergy, the total cost of cooling production also increases, which can be economically challenging.

Fig. 12 shows the changes in the f_{ei} and f_{es} indices as a function of ΔT_E. The results indicate that with increasing ΔT_E, the f_{ei} index increases uniformly. From an engineering perspective, this trend suggests that a higher superheat temperature leads to greater EDR in components such as compressors, heat exchangers, and auxiliary elements. In other words, the rise in the evaporator outlet vapor temperature causes the system to operate further from ideal conditions, resulting in greater non-recoverable energy losses, which are directly associated with increased environmental emissions.

Conversely, the f_{es} index, which indicates the share of exergy destruction relative to the total system output exergy, decreases with increasing ΔT_E. From an engineering standpoint, this reduction reflects an improvement in the relative efficiency of system output. That is, although absolute exergy destruction increases, its proportion compared to the total system output exergy declines, implying a better capacity of the system to preserve exergetic efficiency under higher superheat temperature conditions.

These findings highlight that selecting an appropriate range for the superheat temperature at the evaporator outlet plays a crucial role in balancing exergetic efficiency and environmental impacts. Therefore, in the design and optimization of electric vehicle cooling systems, careful consideration must be given to the optimal value of ΔT_E to simultaneously minimize environmental damage and manage energy losses.

Fig. 13 shows the sensitivity of the economic and exergoeconomic indicators of the system to changes in the interest rate. As can be seen, with an increase in the interest rate, the total cost rate ($\dot{C}tot, k$) decreases. This behavior is because, as the interest rate increases, the annual investment cost in exergoeconomic calculations decreases, because the initial capital is depreciated in a shorter period. In contrast, the cooling cost ($Ccooling$) has an increasing trend, indicating that the production cost of each cooling unit is directly affected by financial and economic conditions.

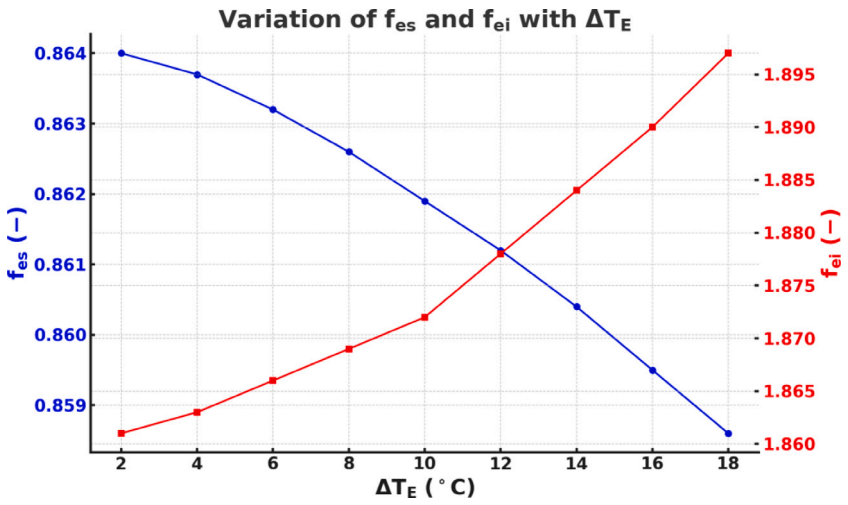

Fig. 12. Variation of f_{es} and f_{ei} of the electric vehicle cooling system concerning ΔT_E.

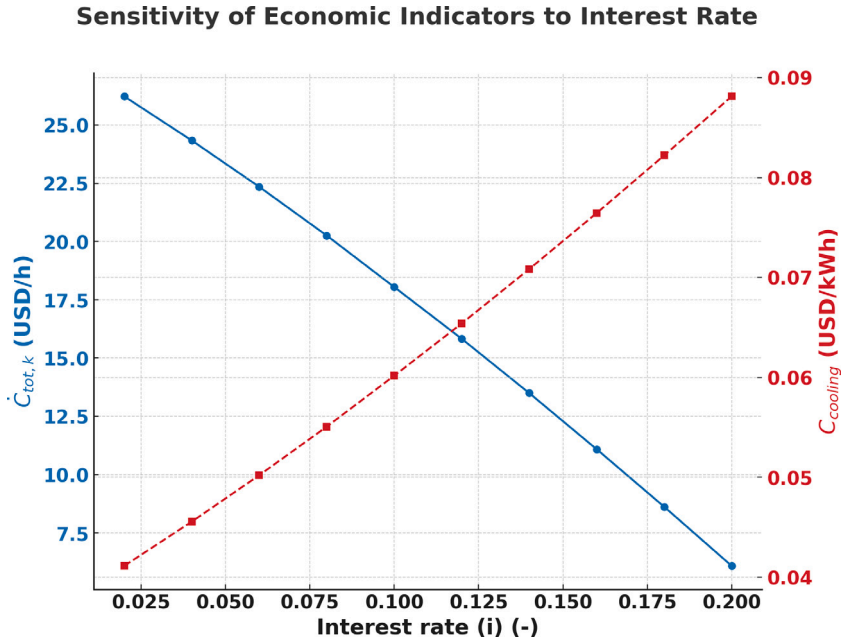

Fig. 13. Sensitivity of cooling cost ($C_{cooling}$) and total cost rate ($\dot{C}_{tot,k}$) to variations in interest rate.

This figure clearly shows that the index $\dot{C}_{tot,k}$, as a main parameter in the exergoeconomic analysis, considers a combination of investment cost and the cost of exergy destruction of components. Therefore, changes in financial assumptions, such as interest rates, can have a significant effect on the distribution of costs among different system components and ultimately affect the results of optimization analysis and design decisions.

Fig. 14 shows that with increasing ambient temperature, both the total cost rate and the exergy destruction rate of the system increase. From an exergy perspective, increasing ambient temperature increases the condensing temperature, the undesirable temperature difference in the exchangers, and also the compressor work, all of which increase entropy production and, as a result, increase exergy destruction. From an exeroeconomic perspective, increasing exergy destruction in the main components of the cycle increases the cost of exergy destruction and directly increases the cost rate of the entire system. Therefore, it is observed that warmer ambient conditions not only reduce the quality of usable energy but also impose a greater economic burden on the system, which highlights the importance of optimizing thermal design and control in such conditions.

3.7. Extension of the study to other working fluids

To conduct comprehensive analyses in the fields of energy, exergy, exergo-economic, exergo-environmental, and economics, in continuation of this research, a preliminary study will be conducted on three alternative refrigerants, including R-152a, R-1234yf, and R-513 A.

The selection of R152a, R1234yf, and R513 A as candidate refrigerants is motivated not only by their thermodynamic performance but also by their environmental and safety characteristics. From an environmental perspective, R134a (the baseline fluid) has a relatively high global warming potential (GWP = 1430), which makes it incompatible with forthcoming EU F-Gas regulations and long-term automotive standards. In contrast, R1234yf is an HFO with an ultra-low GWP of 4,

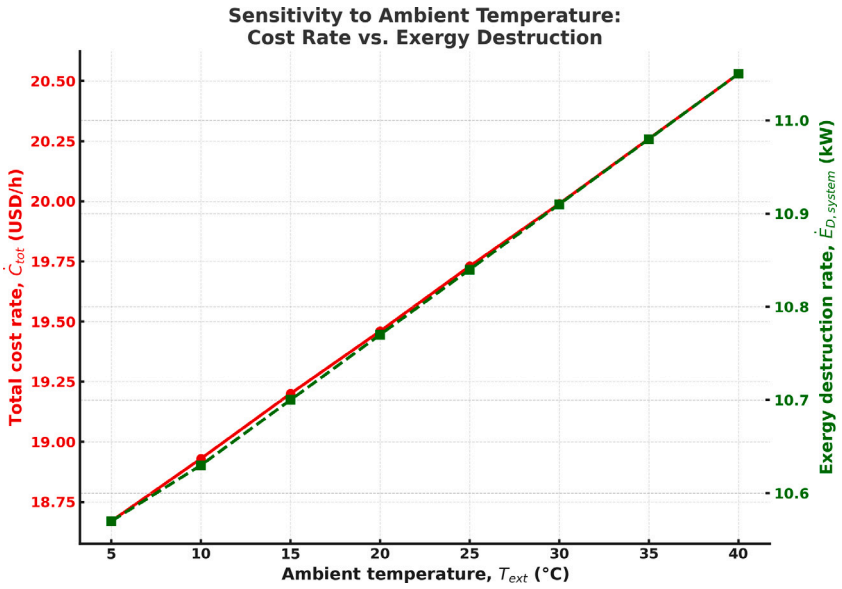

Fig. 14. Comparison of total cost rate and exergy destruction rate of the electric vehicle cooling system under varying ambient temperature (Outdoor temperature).

Table 14
Comparison of thermophysical and environmental properties of R-152a, R-1234yf, and R-513A.

No.	Property	R-152a	R-1234yf	R-513A
1	Molecular weight (g/mol)	66	102	108.4
2	Boiling point (°C)	−24.7	−26.1	−29.2
3	Critical temperature (°C)	113.5	101.1	96.5
4	Critical pressure (bar)	45	40.67	37.65
5	Heat of vaporization (kJ/kg)	279.1	217.2	217.4
6	Specific heat (Liquid, 25°C) (kJ/kg K)	1.803	1.44	–
7	Specific heat (Vapor, 25°C) (kJ/kg K)	1.25	0.85	–
8	Liquid density (25°C) (kg/m^3)	899	1206	1253.3
9	Vapor pressure (25°C) (bar)	4.13	6.661	–
10	Viscosity of liquid (25°C) (cP)	0.160	0.202	–
11	Surface tension (25°C) (mN/m)	–	8.09	–
12	GWP (IPCC AR4)	124	4	573
13	ODP	0	0	0
14	Flammability	Yes	Yes	No

while R152a has a moderately low GWP of 124, and R513 A (a blend of R1234yf/R134a) has a GWP of 573, all of which represent significant reductions compared to R134a. In terms of ozone depletion potential (ODP), all three alternatives have ODP = 0, making them suitable for long-term environmental compliance.

Table 14 shows these working fluids' physical and thermodynamic properties [55–57].

Table 15 shows the results of the calculations of key thermodynamic and economic indicators for four different refrigerants, including R134a, R152a, R1234yf, and R513 A. R152a refrigerant offers the highest efficiency with a COP of 4.0. These differences are due to the thermodynamic properties of these refrigerants and their ability to improve the inlet conditions to the compressor and increase the evaporation capacity in the evaporator.

R152a exhibits a significantly higher latent heat of vaporization compared to R1234yf and R513 A, which increases the cooling capacity per unit mass flow. Moreover, its higher critical temperature reduces irreversibility in the condenser, since the temperature difference during heat rejection becomes smaller. In contrast, R1234yf has a lower latent heat of vaporization and operates with a higher compression ratio due to its lower evaporating pressure. These characteristics increase compressor work input and consequently reduce the COP. The exergy efficiency values for the four refrigerants are quite close to each other, ranging from 5.1% to 5.8%. Although COP shows noticeable variation among the refrigerants, the exergy efficiency does not change significantly because exergy destruction is dominated by components whose irreversibilities are largely insensitive to the refrigerant type. Furthermore, the thermal boundary conditions of the battery and ambient environment do not change with the refrigerant, which limits the extent to which exergy efficiency can improve.

From an economic perspective, the cooling cost (C_{cooling}) for all refrigerants is very close to each other, around 0.055 US$/kWh, indicating that the use of alternative refrigerants does not make a significant difference in terms of operating cost. However, the total capital cost rate ($\dot{C}_{\text{tot},k}$) shows significant differences. R1234yf refrigerant has the highest capital cost rate with 21.6 US$/h, while R152a has the lowest with 18.72 US$/h. These differences can be due to differences in the technical needs of the equipment, safety requirements and costs associated with the design of specific systems for each refrigerant.

Finally, the comparison of the exergoenvironmental indices (exergoenvironmental index $f_{ei,\text{sys}}$ and sustainability index $f_{es,\text{sys}}$) shows that these values are very close for all refrigerants. The values of the exergoenvironmental index range from 1.83 to 1.87 and the sustainability index range from 0.86 to 0.87. These results indicate that although refrigerant substitution can affect the thermodynamic and economic performance of the system, its impact on environmental indicators is less noticeable due to the overall similarity of exergy performance and the proximity of environmental losses. However, in terms of global warming potential (GWP), alternative refrigerants, especially R1234yf, have significant advantages over R134a, which is of great importance in holistic environmental analyses.

Safety considerations are also of great importance: according to the ASHRAE classification, R152a and R1234yf are classified as mildly flammable (A2L), while R513 A is non-flammable (A1). This difference has direct implications for system design, safety requirements and capital costs. For example, R152a, despite its higher efficiency, may require additional safety measures in automotive applications due to its flammability. In contrast, R513 A, although non-flammable, has a higher Global Warming Potential (GWP) and relatively lower efficiency than R1234yf. R1234yf has been widely used in the automotive sector due to its very low GWP and regulatory acceptance, despite its flammability and higher cost. Therefore, including these three refrigerants in this study not only allows for comparison of thermodynamic and exergo-economic performance but also provides a more balanced

Table 15
Comparison of thermodynamic and exergo-environmental indicators for different refrigerants.

No.	Parameter	Symbol	Unit	R134a	R152a	R1234yf	R513a
1	Coefficient of performance	COP	(-)	3.807	4.0	3.5	3.6
2	Exergy efficiency	η_{ex}	(%)	5.5	5.8	5.1	5.3
3	Cooling cost	$C_{cooling}$	US$/kWh	0.055	0.054	0.056	0.055
4	Total capital cost rate	$\dot{C}_{tot,k}$	US$/h	20.26	18.72	21.6	21.3
5	Exergoenvironmental index	$f_{ei,sys}$	(-)	1.86	1.87	1.83	1.84
6	Sustainability index	$f_{es,sys}$	(-)	0.86	0.87	0.87	0.87

assessment of their environmental impacts, safety classifications, and long-term applicability in electric vehicle cooling systems.

A multi-criteria evaluation highlights the trade-offs among performance, safety, environmental impact, and economic feasibility. R152a offers the highest COP due to superior thermodynamic properties, but requires additional safety measures. R1234yf provides the lowest GWP and strong regulatory acceptance at the cost of reduced efficiency. R513 A delivers a non-flammable alternative with moderate performance and a higher capital cost. Therefore, the optimal refrigerant choice depends on the design priorities of the electric vehicle cooling system, whether efficiency, safety, environmental compliance, or cost is the primary constraint.

4. Conclusions

This study developed and analyzed an integrated thermal management system for electric vehicles that combines a vapor-compression refrigeration cycle with a liquid cooling circuit to simultaneously regulate the operating temperatures of three critical components: the battery, vehicle cabin, and electric motor. A comprehensive 5E framework (energy, exergy, economic, exergoeconomic, and exergoenvironmental analyses) was applied to provide a multidimensional assessment of the system's technical performance, cost structure, and sustainability.

Model validation against experimental data demonstrated high reliability, with deviations below 6% for key indicators such as cabin temperature and coefficient of performance (COP), confirming the suitability of the model for optimization studies and engineering decision-making. Under baseline operating conditions, the system achieved a COP of 3.81 and an exergy efficiency of approximately 5.5%. Exergy analysis revealed that the evaporator and condenser were the dominant sources of irreversibility, accounting for the majority of exergy destruction within the cycle. The cabin cooling load, compressor power, evaporator load, and condenser heat rejection were found to be 3.83 kW, 4.2 kW, 16.1 kW, and 20.2 kW, respectively, clearly identifying the heat exchangers as priority components for performance enhancement.

From an economic perspective, the specific cooling cost was calculated as 0.055 US$/kWh. Capital cost analysis showed that the condenser represented nearly 79% of the total investment cost, followed by the compressor (14%) and evaporator (5%). Consistently, the condenser also exhibited the highest exergy destruction cost rate (13.82 US$/s), highlighting a strong alignment between thermodynamic inefficiencies and economic penalties. These results indicate that improving condenser design – through increased heat transfer area, reduced pressure drop, and advanced materials – can yield simultaneous gains in energy efficiency and cost-effectiveness.

Sensitivity analysis demonstrated that battery state of charge (SOC) and evaporator superheat temperature play a critical role in system performance. Optimal operation was achieved for SOC values between 0.65 and 0.75, ensuring a balance between thermal stability and economic efficiency. In addition, increasing superheat temperature improved both COP and exergy efficiency, with exergy performance showing higher sensitivity, emphasizing the importance of advanced control strategies for real-world operation.

Finally, refrigerant comparison showed that R-152a delivered the highest COP and lowest capital cost, while R-1234yf emerged as the most environmentally favorable option due to its ultra-low global warming potential. R-513 A provided enhanced safety but at the expense of slightly lower energy efficiency. These findings confirm that refrigerant selection should be based on a multi-criteria assessment rather than a single performance indicator.

The outcomes of this study provide clear guidance for the practical design of electric vehicle thermal management systems. First, the combined energy–exergy–economic results demonstrate that the evaporator and condenser are the dominant sources of both exergy destruction and total system cost. Therefore, engineering efforts should prioritize advanced heat exchanger design – such as reducing temperature lift, improving heat transfer area, and minimizing pressure losses – rather than focusing exclusively on compressor efficiency. Moreover, the strong dependence of cooling cost and exergy destruction on the battery state of charge indicates that thermal management strategies should be coordinated with the battery management system to favor operation within mid-SOC ranges (approximately 0.65–0.75), where both thermodynamic and economic performance are optimal. Finally, refrigerant selection should be treated as a multi-criteria engineering decision. While high COP is important, safety classification and environmental compatibility (particularly global warming potential constraints) must be considered simultaneously to ensure regulatory compliance and robust real-world implementation.

Future research will extend the present framework by incorporating dynamic and transient simulations under real driving cycles, such as WLTC and US06, to capture rapid load variations during acceleration, braking, and stop–go operation. In addition, integration of the proposed thermal management model with advanced control strategies, including model predictive control (MPC), need to be investigated to enable real-time optimization of energy, exergy, and economic performance. Finally, coupling the 5E framework with a comprehensive life-cycle assessment (LCA) will allow evaluation of long-term environmental impacts and support sustainability-oriented design decisions for electric vehicle thermal systems.

Nomenclature

Symbols

A	Heat transfer surface area [m^2]
A_b	Base (unfinned) surface area [m^2]
A_t	Total surface area (base + fins) [m^2]
A_{cond}	Condenser surface area [m^2]
A_{evap}	Evaporator surface area [m^2]
$A_{bat,channel}$	Battery cooling channel area [m^2]
A_{window}	Window surface area [m^2]
A_{fins}	Added fin area [m^2]
BSA	Body surface area [m^2]
Bo	Boiling number [–]
C	Cost [USD]
$\dot{C}$	Cost flow rate [USD/s]
$\dot{C}_{q,k}$	Thermal exergy cost rate for component k [USD/s]
$\dot{C}_{i,k}$, $\dot{C}_{e,k}$	Inlet/exit exergy cost rate [USD/s]

$\dot{C}_{w,k}$	Cost rate of work for component k [USD/s]
$\dot{C}_{D,k}$	Cost rate of exergy destruction [USD/s]
$\dot{C}_{\text{tot},k}$	Total exergoeconomic cost rate [USD/s]
c	Unit exergy cost [USD/kWh]
c_q	Unit cost of thermal exergy [USD/kWh]
c_w	Unit cost of work exergy [USD/kWh]
c_i, c_e	Unit cost of inlet/outlet flows [USD/kWh]
c_f	Cost per unit exergy destruction [USD/kWh]
C_{pump}	Pump cost coefficient (power-based) [–]
COP	Coefficient of Performance [–]
CRF	Capital Recovery Factor [–]
D_h	Hydraulic diameter [m]
e	Specific exergy [kJ/kg]
e_i, e_e	Specific inlet/exhaust exergy [kJ/kg]
E	Energy [kWh]
$\dot{E}_d$	Exergy destruction rate [kW]
$\dot{E}_q$	Exergy rate associated with heat transfer [kW]
$\dot{E}_{\text{cooling,annual}}$	Annual cooling energy [kWh/year]
f	Rolling resistance coefficient [–]
F	Force [N]
f_r	Darcy friction factor [–]
f_k	Exergoeconomic factor [–]
f_{ei}	Exergy-environmental factor [–]
f_{es}	Exergy stability factor [–]
g	Gravitational acceleration [m/s^2]
G_1	Refrigerant mass flux [kg/m^2 s]
h	Specific enthalpy [kJ/kg] or heat transfer coefficient [W/m^2 K]
h_v, h_l	Enthalpy of saturated vapor/liquid [kJ/kg]
h_{sub}	Subcooled liquid heat transfer coefficient [W/m^2 K]
$\dot{m}$	Mass flow rate [kg/s]
$\dot{m}_i, \dot{m}_e$	Inlet/outlet mass flow rate [kg/s]
k	Thermal conductivity [W/m K]
k_{fin}	Fin thermal conductivity [W/m K]
L_{fin}	Fin length [m]
m_{vehicle}	Vehicle mass [kg]
m_f	Fin shape parameter [m^{-1}]
Nu	Nusselt number [–]
Nu_{tp}	Two-phase Nusselt number [–]
Nu_{lo}	Liquid-only Nusselt number [–]
P	Pressure [Pa]
P_{crit}	Critical pressure [Pa]
Pr	Prandtl number [–]
Φ_{solar}	Solar radiation intensity [W/m^2]
$\dot{Q}$	Heat transfer rate [W]
$\dot{Q}_{\text{cab}}$	Total cabin heat gain [W]
$\dot{Q}_{\text{rad}}$	Solar radiation heat gain [W]
$\dot{Q}_{\text{human}}$	Metabolic heat of passengers [W]
$\dot{Q}_{\text{electric}}$	Electrical devices heat gain [W]
$\dot{Q}_{\text{con}}$	Convective heat gain [W]
$\dot{Q}_{\text{battery}}$	Battery heat generation [W]
$\dot{Q}_{\text{mot}}$	Engine heat generation [W]
R_i	Internal resistance of battery cell [Ω]
Re	Reynolds number [–]
SOC	State of charge [–]
T	Temperature [°C or K]
$T_{\text{cab}}, T_{\text{ext}}$	Cabin/Ambient temperature [°C]
U	Overall heat transfer coefficient [W/m^2 K]
V	Velocity (linear) [m/s or km/h]
$\dot{W}$	Power [kW]
$\dot{W}_{\text{comp}}$	Compressor power input [kW]
$\dot{W}_{\text{pump}}$	Pump power [kW]
x_{tp}	Vapor quality in two-phase flow [–]
Z	Investment cost [USD]
Z_0	Initial investment cost [USD]
Z_n	Updated cost with inflation [USD]
Z_k	Component investment cost [USD]

Greek symbols

α	Thermal diffusivity [m^2/s]
δ	Rotating mass correction coefficient [–]
ε	Effectiveness of heat exchanger [–]
η	General efficiency [–]
η_s	Isentropic efficiency of compressor [–]
η_f	Fin efficiency [–]
η_o	Overall surface efficiency (finned) [–]
η_{mot}	Engine efficiency [–]
η_{ex}	Exergy efficiency [–]
ϕ_{ei}	Environmental damage index (EDE) [–]
f_{ei}	Exergy-environmental factor [–]
f_{es}	Exergy stability factor [–]
m_f	Fin parameter [m^{-1}]
ΔT	Temperature difference [K]
ΔT_{lm}	Logarithmic mean temperature difference (LMTD) [K]

Subscripts

0	Reference (dead) state
1–6	State points of refrigeration cycle
air	Air side
bat	Battery
cab	Cabin
comp	Compressor
cond	Condenser
crit	Critical value
elec	Electrical
evap	Evaporator
ext	External
fins	Fin surface
human	Human-related
in, out	Inlet, Outlet
lo	Liquid-only
mot	Engine
passenger	Passenger-related
pump	Pump
rad	Solar radiation
ref	Refrigerant
solar	Solar-related
sys	System
tp	Two-phase
window	Window surface

Abbreviations

AH	Ampere-hour
BTMS	Battery Thermal Management System
BSA	Body Surface Area
COP	Coefficient of Performance
CRF	Capital Recovery Factor
EDR	Exergy Destruction Rate
EDE	Environmental Damage Effectiveness
ESF	Exergy Stability Factor
EV	Electric Vehicle
EXV	Expansion Valve
HEV	Hybrid Electric Vehicle
HVAC	Heating, Ventilation, and Air Conditioning
LMTD	Logarithmic Mean Temperature Difference
PCM	Phase Change Material

PCS	Phase Change Slurry
TMS	Thermal Management System
O&M	Operation and Maintenance
OCV	Open Circuit Voltage
SOC	State of Charge
TMS	Thermal Management System

CRediT authorship contribution statement

Mehdi Aliehyaei: Writing – review & editing, Writing – original draft, Software, Methodology, Investigation, Formal analysis, Conceptualization. **Vincenzo Bianco:** Writing – review & editing, Writing – original draft, Validation, Supervision, Methodology, Investigation, Conceptualization. **Mattia De Rosa:** Writing – review & editing, Writing – original draft, Validation, Supervision, Methodology, Investigation, Funding acquisition, Formal analysis, Data curation, Conceptualization.

Declaration of competing interest

The authors declare that they have no known competing financial interests or personal relationships that could have appeared to influence the work reported in this paper.

Acknowledgments

This research was funded by the European Union under the LIFE programme (Grant agreement ID: 101167278. RESSKILL project).

Data availability

Data will be made available on request.

References

[1] H. Hamut, I. Dincer, G. Naterer, Exergy analysis of a TMS (thermal management system) for range-extended EVs (electric vehicles), Energy 46 (1) (2012) 117–125, Energy and Exergy Modelling of Advance Energy Systems.
[2] M. Yao, Y. Gan, J. Liang, D. Dong, L. Ma, J. Liu, Q. Luo, Y. Li, Performance simulation of a heat pipe and refrigerant-based lithium-ion battery thermal management system coupled with electric vehicle air-conditioning, Appl. Therm. Eng. 191 (2021) 116878.
[3] W. Xie, X. Liu, R. He, Y. Li, X. Gao, X. Li, Z. Peng, S. Feng, X. Feng, S. Yang, Challenges and opportunities toward fast-charging of lithium-ion batteries, J. Energy Storage 32 (2020) 101837.
[4] B. Liu, Y. Su, Q. Deng, S. Jin, Y. Chen, T. Ouyang, Reducing lithium-ion battery thermal runaway risk based on an integrated cooling strategy for electric vehicles, Int. J. Heat Mass Transfer 216 (2023) 124594.
[5] D.P. Abraham, D.W. Dees, J. Christophersen, C. Ho, A.N. Jansen, Performance of high-power lithium-ion cells under pulse discharge and charge conditions, Int. J. Energy Res. 34 (2) (2010) 190–203.
[6] S. Al Hallaj, H. Maleki, J. Hong, J. Selman, Thermal modeling and design considerations of lithium-ion batteries, J. Power Sources 83 (1) (1999) 1–8.
[7] N. Adhikari, R. Bhandari, P. Joshi, Thermal analysis of lithium-ion battery of electric vehicle using different cooling medium, Appl. Energy 360 (2024) 122781.
[8] S.M. Parsa, F. Norozpour, S. Shoeibi, A. Shahsavar, S. Aberoumand, M. Afrand, Z. Said, N. Karimi, Lithium-ion battery thermal management via advanced cooling parameters: State-of-the-art review on application of machine learning with exergy, economic and environmental analysis, J. Taiwan Inst. Chem. Eng. 148 (2023) 104854, Optimisation in Energy and Process Engineering.
[9] J. Jaguemont, J. Van Mierlo, A comprehensive review of future thermal management systems for battery-electrified vehicles, J. Energy Storage 31 (2020) 101551.
[10] Z. Esmaeili, M. Khoshvaght-Aliabadi, Thermal management and temperature uniformity enhancement of cylindrical lithium-ion battery pack based on liquid cooling equipped with twisted tapes, J. Taiwan Inst. Chem. Eng. 148 (2023) 104671, Optimisation in Energy and Process Engineering.
[11] M. Tousi, A. Sarchami, M. Kiani, M. Najafi, E. Houshfar, Numerical study of novel liquid-cooled thermal management system for cylindrical li-ion battery packs under high discharge rate based on ago nanofluid and copper sheath, J. Energy Storage 41 (2021) 102910.
[12] J. Kim, J. Oh, H. Lee, Review on battery thermal management system for electric vehicles, Appl. Therm. Eng. 149 (2019) 192–212.
[13] M. Lu, X. Zhang, J. Ji, X. Xu, Y. Zhang, Research progress on power battery cooling technology for electric vehicles, J. Energy Storage 27 (2020) 101155.
[14] Y. Lee, W.-S. Kim, J. Han, Comparative study of thermal management systems in electric vehicles: Exergy and energy efficiency under cold climate conditions, Renew. Energy (2025) 123926.
[15] H. Togun, A. Basem, J.M. dhabab, H.I. Mohammed, A.M. Sadeq, N. Biswas, T. Abdulrazzaq, H.A. Hasan, R.Z. Homod, P. Talebizadehsardari, A comprehensive review of battery thermal management systems for electric vehicles: Enhancing performance, sustainability, and future trends, Int. J. Hydrog. Energy 97 (2025) 1077–1107.
[16] J. Wang, L. Ruan, Performance investigation of integrated thermal management system based on a pumped two-phase cooling system for electric vehicles, J. Energy Storage 72 (2023) 107922.
[17] S. Wankhede, A.D. Pingale, A. Kale, Experimental investigation on thermal management of lithium-ion battery pack for formula student electric vehicle using air-cooling system, Energy Storage Sav. 4 (1) (2025) 38–47.
[18] H. Pandey, N.K. Gupta, S.K. Ghosh, Thermo-structural optimization of air-cooling battery thermoregulation system using surrogate modelling and NSGA-II, Therm. Sci. Eng. Prog. 59 (2025) 103270.
[19] R. Habash, G.G. ilis, Ş. Ünal, B.B. Saha, Enhancing COP of electric vehicle cooling systems using adsorption heat pumps, Therm. Sci. Eng. Prog. 64 (2025) 103788.
[20] K. Kumar, J. Sarkar, S.S. Mondal, Energy, exergy, and economic evaluations of various cylindrical lithium-ion battery thermal management systems, Int. Commun. Heat Mass Transfer 165 (2025) 109007.
[21] S. Zong, J. Ren, Y. Guan, Y. Zhang, Z. Cao, X. Yin, X. Yang, F. Cao, F. Duan, Experimental study and performance evaluation of R744 thermal management systems with enhanced parallel cooling for electric vehicles, J. Power Sources 621 (2024) 235152.
[22] P. Song, Z. An, M. Wei, X. Sun, Y. Zhao, D. Dan, Y. Zhang, Cooling performance and optimization of a thermal management system based on CO2 heat pump for electric vehicles, Energy Convers. Manage. 306 (2024) 118299.
[23] A. Wahab, N. Cifterler, N. Amjady, A. Date, H. Kemper, H. Khayyam, Enhancing energy and thermal efficiency of single-phase liquid immersion cooling systems for lithium-ion batteries in electric vehicles, J. Energy Storage 131 (2025) 117365.
[24] A. Sadar, M. Amir, N. Mohammad, An optimal design of battery thermal management system with advanced heating and cooling control mechanism for lithium-ion storage packs in electric vehicles, J. Energy Storage 99 (2024) 113421.
[25] A. Adeniran, J. Bak, B. Bhatia, S. Park, Optimizing single-phase immersion cooling system for lithium-ion battery modules in electric vehicles: A multi-objective design approach, Int. J. Therm. Sci. 210 (2025) 109636.
[26] G. Wu, H. Wu, B. Huang, W. Zhu, Hybrid thermal management system of lithium-ion batteries combing phase change material with liquid cooling under high-rate operation, Int. J. Therm. Sci. 218 (2025) 110117.
[27] J. Wu, F. Jiang, H. Song, C. Liu, B. Lu, Analysis and validation of transient thermal model for automobile cabin, Appl. Therm. Eng. 122 (2017) 91–102.
[28] J. Guo, F. Jiang, A novel electric vehicle thermal management system based on cooling and heating of batteries by refrigerant, Energy Convers. Manage. 237 (2021) 114145.
[29] D.D. Bois, E.F.D. Bois, Clinical calorimetry: Tenth paper—a formula to estimate the approximate surface area if height and weight be known, Arch. Intern. Med. 17 (6) (1916) 863–871.
[30] ASHRAE, ASHRAE handbook – fundamentals, in: American Society of Heating, Refrigerating and Air-Conditioning Engineers, Inc., Physiological Principles, Comfort, and Health, Atlanta, GA, 2017, Chapter.
[31] T. Wang, X. Wu, S. Xu, H. Hofmann, J. Du, J. Li, M. Ouyang, Z. Song, Performance of plug-in hybrid electric vehicle under low temperature condition and economy analysis of battery pre-heating, J. Power Sources 401 (2018) 245–254.
[32] H. Wang, T. Tao, J. Xu, X. Mei, X. Liu, P. Gou, Cooling capacity of a novel modular liquid-cooled battery thermal management system for cylindrical lithium ion batteries, Appl. Therm. Eng. 178 (2020) 115591.
[33] D. Bernardi, E. Pawlikowski, J. Newman, A general energy balance for battery systems, J. Electrochem. Soc. 132 (1) (1985) 5.
[34] F.P. Incropera, D.P. DeWitt, Fundamentals of Heat and Mass Transfer, fourth ed., John Wiley & Sons, Inc., New York City, New York, 1996.
[35] A. Bejan, G. Tsatsaronis, M.J. Moran, Thermal Design and Optimization, Wiley-Interscience, 1996.
[36] T.A.H. Ratlamwala, I. Dincer, M.A. Gadalla, Comparative environmental impact and sustainability assessments of hydrogen and cooling production systems, in: Causes, Impacts and Solutions To Global Warming, Springer New York, New York, NY, 2013, pp. 389–408.
[37] N. Javani, I. Dincer, G. Naterer, B. Yilbas, Exergy analysis and optimization of a thermal management system with phase change material for hybrid electric vehicles, Appl. Therm. Eng. 64 (1) (2014) 471–482.

[38] T.A.H. Ratlamwala, I. Dincer, B.V. Reddy, Exergetic and environmental impact assessment of an integrated system for utilization of excess power from thermal power plant, in: Causes, Impacts and Solutions To Global Warming, Springer New York, New York, NY, 2013, pp. 803–824.
[39] A. Midilli, I. Dincer, Development of some exergetic parameters for PEM fuel cells for measuring environmental impact and sustainability, Int. J. Hydrog. Energy 34 (9) (2009) 3858–3872.
[40] A. Valero, M.A. Lozano, L. Serra, G. Tsatsaronis, J. Pisa, C. Frangopoulos, M.R. von Spakovsky, CGAM problem: Definition and conventional solution, Energy 19 (3) (1994) 279–286, Invited Papers on Exergoeconomics.
[41] R. Selbaş, Ö. Kızılkan, A. Şencan, Thermoeconomic optimization of subcooled and superheated vapor compression refrigeration cycle, Energy 31 (12) (2006) 2108–2128.
[42] S. Sanaye, B. Niroomand, Thermal-economic modeling and optimization of vertical ground-coupled heat pump, Energy Convers. Manage. 50 (4) (2009) 1136–1147.
[43] D. Al-Otaibi, I. Dincer, M. Kalyon, Thermoeconomic optimization of vapor-compression refrigeration systems, Int. Commun. Heat Mass Transfer 31 (1) (2004) 95–107.
[44] R. Hensley, J. Newman, M. Rogers, Battery technology charges ahead, McKinsey and Company report, McKinsey & Company, 2012.
[45] M.S. Peters, K.D. Timmerhaus, R.E. West, Plant Design and Economics for Chemical Engineers, McGraw-Hill, 2003.
[46] S. Leibson, Driving the Chevy Volt, 2012, Posted on August 4, 2012 http://low-powerdesign.com.
[47] E. Bellos, S. Pavlovic, V. Stefanovic, C. Tzivanidis, B. Nakomcic-Smaradgakis, Parametric analysis and yearly performance of a trigeneration system driven by solar-dish collectors, Int. J. Energy Res. 43 (4) (2019) 1534–1546.
[48] C. Tzivanidis, E. Bellos, K. Antonopoulos, Energetic and financial investigation of a stand-alone solar-thermal organic rankine cycle power plant, Energy Convers. Manage. 126 (2016) 421–433.
[49] S. Makkeh, A. Ahmadi, F. Esmaeilion, M. Ehyaei, Energy, exergy and exergoeconomic optimization of a cogeneration system integrated with parabolic trough collector-wind turbine with desalination, J. Clean. Prod. 273 (2020) 123122.
[50] A. Ahmadi, D. Jamali, M. Ehyaei, M. Assad, Energy, exergy, economic and exergoenvironmental analyses of gas and air bottoming cycles for production of electricity and hydrogen with gas reformer, J. Clean. Prod. 259 (2020) 120915.
[51] H.S. Hamut, Exergy and Exergoeconomic Analyses and Optimization of Thermal Management Systems in Electric and Hybrid Electric Vehicles (Ph.D. thesis), University of Ontario Institute of Technology, Oshawa, Ontario, Canada, 2012.
[52] A. Lazzaretto, G. Tsatsaronis, SPECO: A systematic and general methodology for calculating efficiencies and costs in thermal systems, Energy 31 (8) (2006) 1257–1289.
[53] G. Tsatsaronis, Definitions and nomenclature in exergy analysis and exergoeconomics, Energy 32 (4) (2007) 249–253, ECOS 05. 18th International Conference on Efficiency, Cost, Optimization, Simulation, and Environmental Impact of Energy Systems.
[54] S. Bahrami, H.M. Beigi, M.H. Sabour, Experimental analysis of internal heat exchanger for automotive a/c system, in: Proceedings of the ASME 2010 10th Biennial Conference on Engineering Systems Design and Analysis, ESDA, ASME, Istanbul, Turkey, 2010.
[55] S. Sinteco, R-152a Refrigerant Technical Data Sheet, Rev.4, 2025, (Accessed: 3 May 2025) https://www.sinteco-srl.com/wp-content/uploads/2025/01/R-152a-rev4.pdf.
[56] Gas Servei, Technical data sheet: R-1234yf, 2024, (Accessed: 3 May 2025) https://gas-servei.com/wp-content/uploads/2024/06/Technical-data-sheet-R-1234yf-Gas-Servei-1.pdf.
[57] Chemours Opteon, Opteon™ XP10 (r-513a) thermodynamic properties, 2025, (Accessed: 3 May 2025) https://www.opteon.com/es/-/media/files/opteon/opteon-xp10-thermo-properties-si.pdf.